Temporal and spatial variations in benthic nitrogen cycling in a temperate macro-tidal coastal ecosystem: Observation and modeling

Widya Ratmaya, Anniet M. Laverman, Christophe Rabouille, Zahra Akbarzadeh, Françoise Andrieux-Loyer, Laurent Barillé, Anne-Laure Barillé, Yoann Le Merrer, Philippe Souchu

Temporal and spatial variations in benthic nitrogen cycling in a temperate macro-tidal coastal ecosystem: Observation and modeling

Ratmaya Widya [1, *], Laverman Anniet M. [2], Rabouille Christophe [3], Akbarzadeh Zahra [4], Andrieux-Loyer Francoise [5], Barillé Laurent [6], Barillé Anne-Laure [7], Le Merrer Yoann [1], Souchu Philippe [1]

[1] Ifremer , LER MPL, Rue de l'Ile d'Yeu, BP 21105, 44311, Nantes, Cedex 03, France
[2] Université de Rennes, CNRS, UMR 6553 ECOBIO, Campus Beaulieu, 263 avenue du Général Leclerc, Rennes F, 35042, France
[3] Laboratoire des Sciences du Climat et de l'Environnement, CEA-CNRS UNMR 1572, Av. de la Terrasse, 91198, Gif sur Yvette, France
[4] Ecohydrology Research Group, Water Institute and Department of Earth and Environmental Sciences, University of Waterloo, 200 University Avenue West, Waterloo, Ontario, Canada
[5] Ifremer, DYNECO PELAGOS, ZI Pointe du Diable, 29280, Plouzané, France
[6] Université de Nantes, Mer Molécules Santé EA 2160, Faculté des Sciences et des Techniques, BP 92208, 44322, Nantes, Cedex 3, France
[7] Bio-Littoral, Immeuble Le Nevada, 2 Rue du Château de l'Eraudière CS 80693, 44306, Nantes, France

* Corresponding author : Widya Ratmaya, email address : widyaratmaya@gmail.com

Abstract :

We used field observations, laboratory measurements and a reactive transport model (RTM) to investigate temporal and spatial variations in benthic nitrogen (N) cycling in the eutrophic temperate macro-tidal Vilaine Bay (VB), France. A time series of benthic flux measurements and pore-water profiles of dissolved inorganic N (DIN: ammonium, nitrate, nitrite) and dissolved organic N (DON) was conducted at a single station between April and September 2015 (six times). A spatial investigation of the benthic fluxes was performed in July 2016 at this station and three other stations in the VB. All measurements were accompanied by a large panel of physical, chemical and biological descriptors in the water column. In 2015, benthic ammonium fluxes at the monitoring station varied between 75 μmol m−2 h−1 in spring and were less than 10 μmol m−2 h−1 in summer. The benthic DON fluxes co-varied with the ammonium fluxes, ranging from 100 μmol m−2 h−1 in spring to zero in summer. In the summer of 2016, a phytoplankton bloom occurred and as a result the benthic ammonium and DON fluxes reached higher values than in the spring of 2015, accompanied by bottom water hypoxia at one measured station. Benthic nitrate and nitrite fluxes varied between −31 (towards the sediments) and 22 μmol m−2 h−1 and were explained by the bottom water concentration and nitrification rates. After fitting the existing pore-water profiles, the applied RTM correctly simulated the temporal and spatial variations in the benthic DIN fluxes and predicted that a large part of the deposited organic matter (OM) is remineralized aerobically at the sediment-water interface (SWI). The overall results showed a synthetic pattern of benthic N cycling in the VB, based on the occurrence of diatom blooms as the main source of OM in the sediments. The rapid decomposition of this deposited diatom material at the SWI releases large amounts of ammonium and DON to the water

column and rapidly consumes oxygen at the sediment surface. When blooms occur in summer, their decomposition can be followed by hypoxia/anoxia in the bottom water. When blooms are absent, benthic N fluxes are weak and mainly fed by the diffusion from the pore-water. By integrating the present results in a 3D ecological model, it should be possible to more accurately predict the development of bottom water hypoxia in the VB.

Highlights

► The temporal and spatial variations of benthic N cycling in a eutrophic macro-tidal bay are studied using field measurements and the reactive transport model. ► Benthic N flux variations depend on the phytoplankton-derived organic matter input. ► Rapid mineralization of organic matter at the sediment-water interface controls benthic N cycling dynamics and sediment oxygen consumption. ► Organic matter decomposition can be followed by bottom water hypoxia when blooms occur in the summer.

Keywords : DIN, DON fluxes, diatom blooms, hypoxia/anoxia, monitoring station, reactive transport model, sediments

1. Introduction

Coastal areas are among the world's most vulnerable ecosystems to anthropogenic pressures (Turner et al., 2003), particularly to nitrogen and phosphorus pollution which leads to eutrophication (Le Moal et al., 2019). The most visible aspect of anthropogenic marine eutrophication is the mass accumulation of macroalgae on the coast (Smetacek and Zingone, 2013) and phytoplankton blooms (Carstensen et al., 2015). In shallow coastal ecosystems with water bodies exhibiting a residence time of at least several days, senescent phytoplankton blooms can be deposited at the sediment-water interface (SWI) representing a significant amount of oxidizable organic matter (OM) (Smetacek, 1980; Taguchi, 1982). When dead phytoplankton cells decompose, this sometimes results in the depletion of dissolved oxygen (O_2) in bottom waters (Cloern, 2001; Kemp et al., 2005) with a subsequent impact on the ecosystem's structure and function (Gray et al., 2002).

Nitrogen (N) is the key limiting nutrient in many coastal marine environments (Paerl, 2018). In shallow coastal ecosystems, benthic OM remineralization can represent a significant source of N in the water column, helping to maintain eutrophication (Fisher et al., 1982). During algal decomposition in sediment, OM undergoes microbially-mediated biogeochemical transformations, resulting in dissolved organic N (DON) intermediates and dissolved inorganic N (DIN) end products. These can either escape as a benthic flux across the SWI or undergo further transformation in the pore-water (Herbert, 1999; Burdige, 2001). Ammonium (NH_4^+) can be transformed into nitrite (NO_2^-) and nitrate (NO_3^-) under oxic conditions through nitrification (Ward, 2008). Under anoxic conditions, DIN (NH_4^+, NO_3^-, NO_2^-) can be eliminated as N_2 gas through denitrification and/or anammox (Thamdrup and Dalsgaard, 2002; Devol, 2015). The dissimilatory NO_3^- reduction to NH_4^+ (DNRA) competes with denitrification for NO_3^- and tends to retain N in the system (Giblin et al., 2013). The dynamics and competition between these processes govern dissolved N recycling variations and amplitudes at the SWI (Blackburn and Henriksen, 1983; Hulth et al., 2005).

Mechanisms that control benthic N cycling are complex, often site-specific and depend on several factors. These factors include: ambient nutrient concentrations in the water column (Hensen et al., 1998; Khalil et al., 2018), the amount and quality of the deposited OM (Arndt et al., 2013; Ait Ballagh et al., 2021), sediment characteristics (Blackburn and Henriksen, 1983), bottom water O_2 concentrations (Glud, 2008), temperature (Banta et al., 1995) and intensity of the sediment bioturbation (Aller and Aller, 1998), which all vary seasonally. Benthic N cycling can be highly variable over time in coastal ecosystems undergoing phytoplankton blooms (Jensen et al., 1990). In their global synthesis, Boynton et al. (2018) pointed out the lack of time series

measurements for a rigorous evaluation of seasonal and inter-annual variability of oxygen and nutrient exchanges across the SWI in estuarine and coastal ecosystems. More generally, temporal and spatial variations of benthic DIN and DON fluxes in relation with the water column composition, especially chlorophyll *a* (Chl *a*) concentrations as an indicator of phytoplankton biomass, still need to be investigated.

Numerical models are now widely used to simulate phytoplankton blooms and possible hypoxia (or anoxia) under the influence of various nutrient sources and to forecast scenarios of nutrient load reduction for oligotrophication purposes (Ménesguen et al., 2018). Using an ecological model coupled with an early diagenetic model, Soetaert and Middelburg (2009) and Gürevin et al. (2017) have shown how important it is to take benthic nutrient loads into account in order to rehabilitate eutrophic coastal ecosystems. Sedimentary biogeochemical processes must be considered when assessing risks of hypoxia caused by the sedimentation of phytoplankton blooms (Testa et al., 2014). It is therefore essential to understand and quantify how shallow coastal ecosystems accumulate, recycle and eliminate nutrients, especially at the SWI.

Multi-component reactive transport models (RTMs) have been widely used to estimate solute exchange rates at the SWI and biogeochemical processes in both marine and freshwater sediments (Wang and VanCappellen, 1996; Bohlen et al., 2011; Akbarzadeh et al., 2018), but few of these models have been used to simultaneously explore temporal and spatial variations (Paraska et al., 2014). The challenge remains to use a single model (e.g., same reaction parameter values) that could accurately simulate benthic N fluxes and biogeochemical processes as a function of the water column composition, especially phytoplankton biomass and sediment characteristics.

This study aims to investigate the key factors controlling the temporal and spatial variations of benthic N fluxes at the SWI of a macro-tidal coastal bay threatened with eutrophication (i.e., increased phytoplankton biomass). Time-and-space-based field measurement campaigns were accompanied by a large panel of physical, chemical and biological descriptors in the water column. Temporal and spatial datasets were interpreted using a steady-state early diagenetic reactive transport model in order to obtain a general summarized outline of the key processes governing temporal and spatial variations of the benthic N fluxes in the VB.

2. Material and methods

2.1. Study site

The Vilaine Bay (VB) is a shallow macro-tidal coastal bay under direct influence of the Loire and Vilaine rivers (Fig. 1, see Ratmaya et al., 2019 for a detailed description of the riverine nutrient inputs). The VB has a total area of 220 km^2, with a depth varying between 10 and 15 m depending on the tidal amplitude between 4 and 6 m. Water circulation is characterized by low

tidal and residual currents, driven mainly by tides, winds and river flows (Lazure and Jegou, 1998). The water residence time in the bay varies between 10 and 20 days depending on the season and can exceed 30 days during calm periods (Chapelle, 1991). The VB is one of the European Atlantic coastal ecosystems most sensitive to eutrophication (Ménesguen et al., 2019), and has some of the highest concentrations of chlorophyll *a* (Chl *a*) in French coastal waters (Gohin, 2011). In the VB, eutrophication materializes in phytoplankton blooms, characterized by diatom dominance (Ratmaya et al., 2019). The occurrence of phytoplankton blooms in this area is predominantly controlled by the magnitude and timing of river floods (Guillaud et al., 2008) and is simulated using a coupled pelagic biogeochemical and 3D hydrodynamic model (ECOMARS3D; Ménesguen et al., 2019). Oxygen depletion in bottom waters following phytoplankton blooms is frequently observed (Rossignol-Strick, 1985; Ifremer, 2015). Therefore, the onset of hypoxia/anoxia in the VB is probably related to the timing of the phytoplankton blooms induced by river floods. Sediments in the VB are dominated by silt (> 80%), with silty sediments mainly in the north-western part of the bay, silty fine sand sediments in the eastern and north-eastern part of Dumet Island, and rocky substrates (gravels) in the southern part between Dumet Island and Piriac shelf (Le Bris and Glémarec, 1996).

2.2. Sampling strategy

2.2.1. Water column

The water quality in the VB is monitored regularly as part of the French National Observation Network for Phytoplankton and Hydrology (REPHY, Belin et al., 2020) and Water Framework Directive (WFD) at two monitoring stations, Nord Dumet (ND) and Ouest Loscolo (OL; Fig. 1). Surface water at the ND Station has been monitored monthly (at 1 m below the surface) since 2008 as part of REPHY and WFD for the nutrient and Chl *a* concentrations, and phytoplankton composition. This station also benefits from an instrumented buoy (MOLIT), deployed since 2008 to monitor the temperature, salinity, dissolved oxygen and turbidity in surface and bottom waters with an hourly frequency. Surface waters at the OL station has been monitored bi-monthly since 1996 for phytoplankton, nutrients and physical parameters (temperature, salinity, dissolved oxygen) as part of REPHY and WFD.

2.2.2. Sediment

The year 2015 was devoted to a temporal study and involved renewing measurements and experiments at a single station on six dates between April and September and by alternating periods of strong (spring) and weak (neap) tides in order to take tidal variations into account. The ND

153 monitoring station (St. A, Fig. 1) was chosen for its high frequency monitoring of physicochemical
154 parameters.

155 Close to 30 stations spread over the whole bay were sampled in April 2016 to assess the
156 spatial distribution of the sediment granulometry (grain size, porosity, density), organic carbon
157 (C_{org}), total nitrogen (TN), biogenic silica (BSi) and Chl *a* contents in the first 5 cm of the
158 sediments. Spatial variations of the benthic fluxes were measured at four stations (including the
159 ND monitoring station) selected among those sampled in April 2016. All four campaigns were
160 grouped together over a short period to minimize temporal variations (July 18th to 28th).

161 *2.3. Data acquisition*

162 *2.3.1. River discharge*

163 River discharge data were extracted from the French hydrologic "Banque Hydro" database
164 (http://www.hydro.eaufrance.fr/, access: 20 May 2016). Daily discharge data were available at the
165 Montjean-sur-Loire gauging station for the Loire River and at the Rieux gauging station for the
166 Vilaine River.

167 *2.3.2. Water column*

168 Physicochemical (temperature, salinity and dissolved oxygen), phytoplankton and nutrient
169 data from the ND and OL monitoring stations were used to provide a hydrological context for the
170 benthic N flux studied in 2015 and 2016. Additional samples were taken bimonthly at the ND
171 station in bottom waters (1 m above the bottom) from March to October 2015 for the nutrient and
172 Chl *a* analyses. Physicochemical data at the ND station were obtained from the MOLIT buoy, and
173 were validated and published in SEANOE (Retho et al., 2020). Water samples for the DIN and
174 DON analyses were filtered using syringe fitted filters (CA membrane 0.2 µm Sartorius®) and
175 stored at -20°C.

176 *2.3.3. Sediment core sampling and treatments*

177 For each sampling date, 20 undisturbed cores were collected by scuba divers using
178 Plexiglas® tubes (9 cm inner diameter; 30 cm height). Each core contained approximately 15 cm
179 of sediment with 1 L of overlying water. Upon collection, all sediment cores were transported to
180 the laboratory within 2 h.

181 For two sets of the triplicate sediment cores, the top first 15 cm were sliced into 10
182 horizontal layers in a glove box filled with N_2 (1 cm intervals for 0-6 cm, 2 cm intervals for 6-12
183 cm, and 3 cm intervals for 12-15 cm). The first triplicate of the sediment cores was used to extract

the pore-water. For each layer, the pore-water was extracted by centrifugation at 3360 *g* for 20 minutes at in situ temperature. The pore-water was filtered using syringe fitted filters (CA membrane 0.2 µm Sartorius®) and stored at -20°C for the DIN and DON analyses. An aliquot of the sediment remaining after the pore-water was collected for each layer was frozen for the C_{org} and TN analyses.

The second triplicate of the sediment cores was used for the sediment physical property analysis. For the grain size analysis, an aliquot of the wet sediment samples from each layer was stored in a plastic bottle containing a mixture of one third ethanol and two thirds distilled water to prevent microbial activity. Another aliquot of wet sediment of known volume and weight was dried (45°C, 5d) for the density and porosity analysis. For another triplicate of the sediment cores, the top first cm was sliced and frozen for the sediment Chl *a* analysis.

One sediment core was used to measure the vertical profiles of the dissolved O_2 at the SWI and in the sediment using a miniaturized Clark-type oxygen sensor (Unisense OX500®) coupled with a picoammeter (Unisense PA2000®) and a micromanipulator (Unisense MM33®) at room temperature. The position of the SWI was determined visually from the O_2 microprofile according to Lansard et al. (2008), by adjusting the SWI position to the steepest O_2 concentration gradient.

For the spatial study carried out in April 2016, the samples of the first 5 cm of the sediments for the physical property analysis were lost and therefore are not presented here.

2.3.4. Benthic DIN and DON fluxes

For each sampling date and station, approximately 80 L of bottom water was collected using a peristaltic pump for laboratory incubation experiments. When collecting bottom water samples, the light intensity was also measured at 0.5 m above the bottom using a Li-COR Spherical Underwater Quantum Sensor. Benthic fluxes were measured using the sediment core incubation technique. For each experiment, duplicate sediment cores were incubated at in situ temperature and light conditions in a thermo-regulated water bath with one duplicate wrapped with tin foil to avoid light exposure. Two additional cores, containing only bottom water (blank cores), were incubated in order to verify changes in the concentration in the overlying water. Each tube was carefully sealed with a cap equipped with a stirring rod (Fig. S1). The overlying water was gently stirred while avoiding sediment resuspension. During incubation, a probe was used to monitor O_2 in the overlying water in order to make sure that O_2 concentrations did not drop below 20% of the initial sampling values (Dalsgaard et al., 2000). The overlying water was sampled five to six times during the 20 to 24 h incubation period. Water samples were immediately filtered using syringe

fitted filters (CA membrane 0.2 µm Sartorius®) and stored at -20°C for analysis. The sampled volume (50 mL) was replaced with the same volume from a reserve tank containing unfiltered bottom water. Fluxes were calculated from the change in concentrations over the incubation time after a correction for dilution due to replacing the overlying water and possible changes in the blank cores. Only significant slopes (linear regression, $p < 0.05$) were taken into account, otherwise the fluxes were considered to be zero. Finally, the results from light and dark measurements ($n = 4$) were pooled because there was no significant difference between both treatments (Mann-Whitney, $p > 0.05$). At the end of incubation, sediments were fixed using 10% formalin for the macrofauna counts and identification.

2.3.5. Potential nitrification and NO_3^- reduction

Potential nitrification step 1 (NH_4^+ oxidation to NO_2^-) rates were measured by incubating slurries containing sodium chlorate ($NaClO_3$) in order to inhibit NO_2^- oxidation (Bianchi et al., 1994; Gilbert et al., 1997). Fresh sediments (30 g) from the 0-2 cm layer were mixed homogeneously with 1 L of filtered bottom water (CA membrane 0.2 µm Sartorius®) in polycarbonate bottles. A control triplicate of bottles contained untreated slurries only. Two mL of $NaClO_3$ (10 mM) was added to one triplicate of bottles. No substrate was added. Slurries were incubated for 20 to 24 h in the dark at in situ temperature, with loosely fitted caps to ensure oxic conditions. Each slurry was subsampled every 4 h, and subsamples were centrifuged (3920 *g*, 15 min). The supernatant (~10 mL) was sampled, fixed with 50 µL $HgCl_2$ (60 g L^{-1}) and stored at 4°C while awaiting NO_2^- analysis. The rates were calculated using a linear regression of the change in NO_2^- concentrations over time. Only significant slopes (linear regression, $p < 0.05$) were taken into account, otherwise the rates were considered to be zero.

Potential NO_3^- reduction rates were measured using flow-through reactor methods (Laverman et al., 2006). For each experiment, duplicate sediment layers (0-2 cm) were placed in Plexiglas® rings (4.2 cm inner diameter; 2 cm height). A 0.2 µm pore size PVDF (Durapore®) membrane filter and a glass fiber backing filter (1.2 mm thickness, 4.7 cm diameter) were placed at both ends of the ring, and the resulting sediment reactor cell was enclosed by two Plexiglas® caps with in/outflow channels. Reactor cells were fed with a saline solution containing NO_3^- (salinity 33, 4500 µM KNO_3) using a peristaltic pump (Gilson Minipuls®) at a constant flow rate (2 mL h^{-1}). The saline NO_3^- containing the input solution was bubbled with N_2 for about 10 minutes to exchange and replace the existing gas phase creating an anoxic solution. Samples were collected from the outflow of the reactors every 4-6 h during 20 to 24 h. Reduction rates were determined

from the difference in the NO_3^- concentrations at the inflow and outflow, multiplied by the flow rate and normalized by the volume of the reactor.

The measured potential NO_3^- reduction rates (NRR) were corrected for in situ temperature using the Arrhenius equation (eq. 1) and fitted to the Michaelis-Menten rate expression (eq. 2)

$$\text{Pot. NRR}_T = \frac{\text{Pot.NRR}_{Tl}}{\text{Q}_{10}^{\left(\frac{\text{Tl}-\text{T}}{10}\right)}} \quad (1)$$

$$\text{R} = \frac{\text{Pot.NRR}_T * [\text{NO}_3^-]}{\text{k}_{NO} + [\text{NO}_3^-]} \quad (2)$$

where Pot.NRR_T is the potential NRR corrected with in situ temperature *T*, Pot.NRR_{Tl} is the potential NRR measured at laboratory temperature *Tl*, Q_{10} is a temperature coefficient (Q10 = 2.5; Laverman et al., 2006); k_{NO} is the affinity constant of NO_3^- for denitrification (see Table S2), and $[NO_3^-]$ is the average measured NO_3^- concentrations in the first 2 cm of sediment.

2.3.6. Analytical methods

Sediment grain size was measured using the laser diffraction technique (Malvern 2000) on wet sediment samples. Density and porosity were calculated from the weight loss after drying. Sediment C_{org} and TN concentrations were measured on freeze-dried sediment using a Thermo Scientific™ elemental analyzer after eliminating inorganic carbon using phosphoric acid (Cauwet, 1975). The BSi content was determined via the alkaline extraction method using 0.1 M sodium carbonate (Na_2CO_3) at 85°C (DeMaster, 1981). The extract was analyzed as dissolved silica (DSi). NH_4^+, NO_3^-, NO_2^- and DSi concentrations were measured using a segmented flow colorimetric analysis according to Aminot and Kérouel (2007). NO_3^- and NO_2^- concentrations in the water column were reported as the sum of NO_3^- + NO_2^-. Total dissolved N (TDN) concentrations were analyzed using the persulfate oxidation method according to Raimbault et al. (1999) after NH_4^+ removal (Burdige and Zheng, 1998). DON concentrations were determined from the difference between TDN and DIN. Chl *a* concentrations in the water column were measured using spectrophotometry according to Aminot and Kérouel (2004). Sediment Chl *a* concentrations were extracted from freeze-dried sediment according to Lorenzen (1967) after an extraction with 90% acetone and ultrasonication for 5 minutes (Sundbäck et al., 1996). Microscopic observations of the phytoplankton and/or microalgae dominant species in the sediment surface were conducted on Lugol-fixed samples collected from the uppermost mm of sediments.

2.3.7. Data analysis

If not stated otherwise, measurements are reported here as the average ± standard error: triplicate cores for the potential nitrification-denitrification rates and Chl *a* in the sediment surface, and four replicate cores for the benthic fluxes. Variations in the C_{org}, TN, DIN and DON concentration profiles between sampling dates and depths were analyzed using a non-parametric Kruskal-Wallis test. The inter-variable relationship was tested using a linear regression. Spearman's rank correlation was used to analyze the relationship between benthic macrofauna density, N transformation rates and benthic N fluxes for the temporal study carried out in 2015. Bottom water turbidity and O_2 concentrations were also added to take the potential influence of sediment resuspension on benthic N transformation into account. For all tests, the level of significance was set to $p < 0.05$, and these tests were performed using the STATGRAPHIC CENTURION software (Statgraphics Technologies Inc., Version XVIII, Released 2018). The spatial distributions of C_{org}, TN, BSi and Chl *a* in the first 5 cm of sediment were visualized using the Ocean Data View software. Automatic weighted-average gridding was used to spatially interpolate the data (Schlitzer, 2002).

2.4. Reactive transport model

2.4.1. Model description

A one-dimensional steady state reactive transport model (RTM) was applied to the dataset mainly to simulate sediment-water DIN fluxes, as well as DIN concentrations in the pore-water and to quantify N transformation process rates. This present study focuses on the sediment N cycle by integrating a newly developed N reaction network as developed by Akbarzadeh et al. (2018). DON benthic flux modeling was limited to only calculating the diffusive fluxes.

2.4.2. Reactions

This model combines general organic matter (OM) oxidation reactions with N transformation processes. Five principal reactions in the sediment N cycle are considered: ammonification, nitrification, denitrification, dissimilatory NO_3^- reduction to NH_4^+ (DNRA) and anammox (Table S1). NH_4^+ production (ammonification) occurs by aerobic respiration, denitrification, DNRA, dissimilatory iron reduction and sulfate reduction. Nitrification is modeled as a two-step process: NH_4^+ (step 1) and NO_2^- (step 2) oxidation, respectively. Anaerobic processes (denitrification, DNRA, anammox, $Fe(OH)_3$ and SO_4^{2-} reduction) are prevented by the presence of O_2 using an inhibition term (F_{In}). Denitrification and DNRA are modeled as a one-step process of OM oxidation using NO_3^-, with N_2 and NH_4^+ production, respectively, as the ultimate end result. The fraction of the NO_3^- reduction by denitrification and DNRA is assumed to be a fixed value. A term F_{DNRA} is added to distribute the fraction of NO_3^- reduction between two pathways (Canavan

et al., 2007; Akbarzadeh et al., 2018), and the fraction of NO_3^- reduced by denitrification is defined as 1 minus (-) F_{DNRA} (Table S1). The F_{DNRA} value was adjusted by testing a series of values (5, 10, 25, 50, 75, 90, 95%) to obtain the fit of the NH_4^+ fluxes. The retained value was 5% (see Supplement).

2.4.3. Boundary conditions and reaction parameters

NH_4^+, NO_3^-, NO_2^- and O_2 concentrations measured in the bottom water were set as the upper boundary conditions (Table S2). This model considers two pools of organic matter: a labile pool (abbreviated as OM1) and a less labile pool (abbreviated as OM2), as well as the following N species: NH_4^+, NO_3^-, NO_2^-. Additional chemical species include dissolved O_2, sulfate (SO_4^{2-}), dissolved iron (Fe^{2+}) and iron hydroxides ($Fe(OH)_3$). For solid species, deposition fluxes at the SWI were imposed. Measured benthic fluxes for the NH_4^+ and O_2 pore-water profiles were used to constrain the depositional fluxes of OM1, whereas the depositional fluxes of OM2 were adjusted to best reproduce the NH_4^+ and NO_3^- pore-water profiles. A C:N ratio of 10 was assumed for OM1 according to the measured average C:N molar ratio sediment surface (Table S3), while that of OM2 was assumed to be poorer in N (C:N = 15). The lower boundary conditions of all chemical species were set to zero concentration gradients.

The reaction rate parameters detailed in Table S3 were obtained following a common procedure in the early diagenetic modeling (e.g., Wang and VanCappellen, 1996; Canavan et al., 2006; Dale et al., 2011; Akbarzadeh et al., 2018). Values were either taken directly from the literature or adjusted by trial and error to obtain global fits of the model to the DIN pore-water profiles and benthic flux datasets. For further details about the original model and examples of applications, see Canavan et al. (2006), Couture et al. (2010), Torres et al. (2015) and Akbarzadeh et al. (2018).

2.4.4. Transport

Solid chemical species in the simulated sediment column are transported by the sediment advective velocity and particle mixing due to bioturbation, while solute chemical species are additionally transported by molecular diffusion and bioirrigation. The change in concentration for solute (eq. 3) and solid (eq. 4) species is described in the following mass conservation equations:

$$\emptyset \frac{\partial(C_d)}{\partial t} = \emptyset \frac{\partial^2(D_b C_d)}{\partial x^2} + \emptyset \frac{\partial^2(D_s C_d)}{\partial x^2} - \emptyset \omega_d \frac{\partial(C_d)}{\partial x} + \emptyset \alpha (C_{d0} - C_d) + \emptyset \sum R_d = 0 \quad (3)$$

$$(1 - \emptyset)\rho \frac{\partial(C_s)}{\partial t} = (1 - \emptyset)\rho \frac{\partial^2(D_b C_s)}{\partial x^2} - (1 - \emptyset)\rho \omega_s \frac{\partial(C_s)}{\partial x} + (1 - \emptyset)\rho \sum R_s = 0 \quad (4)$$

where C_d and C_s are the solute and solid species concentrations respectively, D_b is the bioturbation coefficient ($cm^2\ yr^{-1}$), D_s is the molecular diffusion coefficient ($cm^2\ yr^{-1}$), α is the bioirrigation coefficient (yr^{-1}), ρ is the sediment dry density ($g\ cm^{-3}$), ω_d and ω_s are the advective or burial velocities of the pore-water and solids, respectively ($cm\ yr^{-1}$), Ø is the sediment porosity, and R_d and R_s are the reaction rates for the solute and solid species, respectively. The D_s values for all solute species included in the model were corrected with the bottom water temperature and sediment porosity for each measurement according to Boudreau (1997). The D_s of DON was estimated using the empirical relationship between the free solution diffusion coefficient (D_o) and molecular weight (MW) for various organic compounds at 25°C in distilled water reported by Burdige et al. (1992), assuming a fixed average MW of 2500 Daltons. The obtained values were then corrected for the in situ temperature using the Stoke-Einstein equation and transformed to D_s after correction for sediment porosity (Boudreau, 1997). Bioturbation and bioirrigation were described in the model by a coefficient with values that decrease with depth (Table S4).

2.4.5. Modelling strategy

The model was run to steady state ($\partial C/\partial t = 0$), although we are aware that coastal sediments are a more transient environment than shelf or deep-sea sediments. The steady state assumption was based on the calculation of diffusion time-scales of solutes calculated from the modified Einstein-Smoluchowski equation (Jørgensen and Revsbech, 1985). If these time-scales are smaller than the elapsed time between two campaigns, it can be assumed that the system has re-equilibrated to the new condition and can be treated in a pseudo steady state. The diffusion time-scales and residence time of DIN (NH_4^+, NO_3^-, NO_2^-) were estimated over the first 2 cm sediment layer, where the exchange of DIN between the sediment and overlying water occurs most actively. They vary from 1 to 3 days (Table S5) and from 2 to 7 days (Table S6) for the diffusion time-scales and residence time, respectively, and were lower than the elapsed time between two campaigns (8-15 d). The diffusion time-scales and residence time for DON were approximately six to eight times greater than those for DIN (Tables S5, S6). A detailed description of the diffusion time-scale calculation is provided in the Supplement.

2.4.6. Spatial simulation

Benthic DIN fluxes measured in July 2016 were simulated using the same fixed parameter values as in 2015 (Tables S3, S4).

2.4.7. Sensitivity analyses

The RTM was also used as a sensitivity tool to identify the main factors (e.g., parameter set, forcing functions) that exert the most effect on benthic DIN fluxes (e.g., increase, decrease or direction change). The set of parameters tested were those related to environmental factors and suspected to have the largest effect on SWI DIN exchanges. These include the depositional fluxes of OM1, its reactivity (k_1 OM1), the proportion of OM1 and OM2, the C:N ratio of OM1, bioturbation (Db), bioirrigation (α) in addition to the bottom water concentration of O_2 and NO_3^- (Table S7). A stepwise approach was applied by manually changing the parameter values individually and observing the model response on the NH_4^+ and NO_3^- fluxes. The model was run by imposing each change in these values one by one for each sampling date of the temporal study in 2015. No combination effects between the parameters were tested in the sensitivity analysis of this present study. The response was calculated as a percentage of change in the NH_4^+ and NO_3^- fluxes with regard to the best fits (baseline model). The contribution of NO_2^- to the DIN fluxes was considered to be negligible (< 5% of the NH_4^+ and NO_3^- fluxes) and therefore they were not included in the sensitivity analysis.

3. Results

3.1. Hydrological conditions in 2015 and 2016

During both studied periods (April-September 2015 and July 2016), the seasonal variations of the physico-chemical parameters in the water column at both monitoring stations in the VB essentially depended on climatic conditions and freshwater inputs from the Loire and Vilaine rivers (Figs. 2, S2). The water column temperature varied between 10°C in March and 21°C in July with temporary stratifications of several degrees in summer. The water column O_2 concentrations exhibited opposite variations to those observed for temperature. The lowest bottom water O_2 concentration value, close to the hypoxia threshold (63 µM, Middelburg and Levin, 2009; Zhang et al., 2010), was detected at St. B in July 2016 (96 µM, Table S2). Discharges from the Loire and Vilaine rivers displayed similar variations in 2015 with a flood in May, while 2016 was characterized by a flood from the Loire River in early June. Within one week after flooding, the surface water in the VB displayed drops in salinity below 28, coinciding with the peaks of $NO_3^- + NO_2^-$ concentrations (> 60 µM). Aside from these peaks, the surface and bottom water $NO_3^- + NO_2^-$ concentrations were ~20 µM in spring and they gradually decreased in June to reach levels below 1 µM. With regards to all four stations studied in July 2016, the highest $NO_3^- + NO_2^-$ concentration was recorded at St. B (Table S2). NH_4^+ concentrations remained below 2 µM in the surface water. Peaks were recorded in the bottom water in May 2015 (> 5 µM) and in June 2016 (> 3 µM), decreasing gradually below 1 µM in July. In 2016, the highest NH_4^+ and minimum O_2 concentrations were found at St. B (Table S2). Chl *a* concentrations in the surface water peaked

(> 15 µg L^{-1}) in March and May in 2015 and in June 2016 corresponding to diatom blooms. Small peaks (~5 µg L^{-1}) of diatom blooms were observed in August 2015 and October 2016 (see Retho, 2019 for additional information). For both studied periods, DON concentrations at the ND station varied around 7 µM throughout the year in both the surface and bottom waters (not shown).

3.2. Sediment characteristics

The sediment grain size distribution at the ND monitoring station was dominated by very fine particles (< 63 µm) and remained constant with depth regardless of the sampling date (Fig. S3). At three stations sampled in July 2016, this distribution was dominated by a very fine fraction (< 63 µm) at St. B, a coarse fraction (> 100 µm) at St. C and gravel at St. D (Fig. S4). Sediment porosity and dry density varied slightly with the depth (0.85-0.79 and 2.96-2.90, respectively) and sampling dates (0.80-0.82 and 2.60-2.96, respectively) at the ND station, and displayed spatial variations according to the grain size distribution (Figs. S5, S6). Sediment C_{org} and TN concentrations at the ND monitoring station were not significantly different according to the date and depth ($p > 0.05$), with median values of 1,168 (~1.6% DW) and 120 µmol g^{-1} (~0.2% DW) for C_{org} and TN, respectively (Figs. 3a, 3b). The median of the C:N molar ratio varied between 9.2 in the first top cm and 10.8 at depth (Fig. 3c). C_{org}, TN and BSi concentrations at the sediment surface (5 cm) ranged respectively from 221 to 2,095, 25 to 233, and 10 to 215 µmol g^{-1} and were higher in the north-western part of the bay than in the south-eastern part (Fig. S7).

At the ND monitoring station in 2015, the Chl *a* content in the first cm of sediment slightly increased from 8.9 ± 1.4 µg g^{-1} in April to 11.9 ± 1.5 µg g^{-1} in June (Fig 2d), it decreased in August (4.6 ± 0.3 µg g^{-1}) and then slightly increased in September (8.7 ± 0.9 µg g^{-1}). The highest values in April and June were found subsequent to spring diatom blooms. Benthic Chl *a* displayed a spatial variation similar to that of C_{org}, TN and BSi (Fig. S7), with the highest concentration observed at St. B (Fig. 2h). Microscopic observations of the sediment surface in 2015 revealed abundant benthic diatoms (*Pleurosigma* sp., *Navicula* spp., *Nitzschia* spp.) and organic debris in April and June, while there was less organic debris, some phytoplanktonic (*Thalassiosira* sp.) and tychoplanktonic (*Paralia* sp.) diatoms and many empty cells in August and September (Fig. S9). Overall, on average, the macrofauna density in the incubated sediment cores of the ND monitoring station in 2015 were < 1,500 ind. m^{-2}, dominated by *Nucula nitidosa* (a small bivalve), *Amphiura filiformis* (a brittle star) and *Sternaspis scutata* (polychaeta) (Table S8). No significant correlations were observed between the benthic macrofauna density and benthic N transformation rates, and measured N fluxes (Table S9).

3.3. Oxygen and dissolved N pore-water profiles

Irrespective of the sampling date, the O_2 concentration decreased rapidly within the first 2 mm and was undetectable below this depth (Fig. 4a). In 2015, pore-water NH_4^+ concentrations at the ND station showed positive concentration gradients in the first 5 cm (Fig. 4b) and nearly constant values around 300 µM below 5 cm, except in two cores (June 24th and August 5th with a value exceeding 1200 µM). NH_4^+ concentration profiles did not show any significant differences between sampling dates ($p > 0.05$). In 2015, pore-water DON concentrations at the ND station were higher than those in the bottom water, with no significant difference between sampling dates ($p > 0.05$, Fig. S8a). Steep positive concentration gradients were observed in the top 1 cm, which became weaker in the layer below. The global mean pore-water DON concentration was higher than that of NH_4^+ in the first 5 cm layer and lower below (Fig. S8b). Pore-water NO_3^- concentrations at the ND station displayed negative concentration gradients in April 2015 (Fig. 4c). Peaks of NO_3^- were observed in the top first 0.5 cm from June to September 2015, with a high value up to 12 µM on August 5th. Pore-water NO_2^- concentrations were low (< 2 µM). Peaks of NO_2^- maxima were generally observed in the first 1 cm, which decreased gradually below (Fig. 4d).

3.4. Dissolved N fluxes at the SWI

NH_4^+ fluxes measured at the ND station in 2015 varied between 36 ± 22 µmol m^{-2} h^{-1} in April and 50 ± 19 µmol m^{-2} h^{-1} in June (Fig. 5a), and were 10 times lower in August and September (5.3 ± 4.5 µmol m^{-2} h^{-1}). Maximum NH_4^+ fluxes were found after spring blooms, as observed for the sediment Chl *a* content (Fig. 2d). The calculated diffusive NH_4^+ fluxes, based on pore-water concentration gradients in the first cm measured in 2015, were approximately 50% of the measured fluxes, with little variation over time (Table S6). In 2016, NH_4^+ fluxes were three times higher than those measured in June 2015 and displayed spatial variation, with maximum values observed at St. A and St. B. NH_4^+ fluxes measured at the ND station in 2015 were positively correlated to the Chl *a* content in the first cm sediment layer ($r = 0.82$, $p < 0.05$, Fig. 6a). Benthic DON fluxes measured at the ND station in 2015 had similar values and displayed a temporal variation similar to those of NH_4^+ (Fig. 5b), with which they were positively correlated ($r = 0.82$, $p < 0.05$, Fig. 6b). DON fluxes were close to zero in August and September. In 2016, the DON fluxes were in the same order of magnitude as those measured in 2015. Diffusive DON fluxes represented approximately 10% of the measured DON fluxes in spring and were higher in summer than in spring, with little variation over the sampling dates (Table S6). At the ND station, NO_3^- fluxes were directed towards the sediments in April 2015, with an average rate of -17 ± 5 µmol m^{-2} h^{-1} (Fig. 5c), coinciding with high NO_3^- concentrations in the bottom water (Fig. 2c). For the rest of the studied period, NO_3^- was released from the sediments except in August 2015 when the values

were close to zero (< 0.1 µmol m^{-2} h^{-1}). The release of NO_3^- represented approximately 25% of the NH_4^+ fluxes. In 2016, the measured NO_3^- fluxes varied between the stations, with a flux towards the sediments particularly at St. B (Fig. 5c), coinciding with high bottom water NO_3^- concentrations (Table S2). The measured NO_2^- fluxes remained below 5.0 µmol m^{-2} h^{-1}, maximum values were observed in June and September in 2015 and there was a flux towards the sediments at St. B in 2016 (Fig. 5d). For all benthic flux values, there was no significant difference between measurements during spring and neap tides (Mann-Whitney, $p > 0.05$).

3.5. Potential nitrification and NO_3^- reduction rates

In 2015, the potential rates of nitrification measured at the ND station increased from April to June (11.5 ± 0.4 to 28.0 ± 2.9 µmol N m^{-2} h^{-1}) and then decreased afterwards in August (14.0 ± 2.5 µmol N m^{-2} h^{-1}) and September (12.0 ± 1.3 µmol N m^{-2} h^{-1}) to values comparable to those in April (Table 2). The potential nitrification rates measured in July 2016 were lower than those measured in 2015. The potential NO_3^- reduction rates measured in 2015 increased from April (52.4 ± 6.6 µmol N m^{-2} h^{-1}) to their maximum values in June (119.0 ± 24.8 µmol N m^{-2} h^{-1}; Table 2).

3.6. Model outputs

3.6.1. Organic matter mineralization and N transformation rates

Aerobic respiration was the major pathway of labile OM (OM1) mineralization (Table 1), with rates displaying similar temporal and spatial variations to those for OM1 depositional fluxes (Table S2). Aerobic respiration represented up to 75% of the total rates. The anaerobic OM mineralization pathway was dominated by SO_4^{2-} reduction, with the highest value at St. B in 2016. The reduction of NO_3^- and $Fe(OH)_3$ activities was less significant (~10% of the total rates for both processes). The modeled nitrification rates (step 1) were similar to the measured potential rates and displayed similar temporal and spatial variations (Table 2). In 2015, the model-predicted denitrification rates revealed a temporal variation contrary to the measured potential rates and model-predicted nitrification rates, with the highest rates in April decreasing over the studied period. In 2016, St. B displayed the highest denitrification rates. Adjusting the F_{DNRA} value to 5% of all of the reduced NO_3^- resulted in the best fit of the NH_4^+ fluxes. When values higher than 5% were tested, this resulted in an overestimation of the NH_4^+ fluxes (Fig. S10). The anammox rates were quantitatively low (< 0.2 µmol m^{-2} h^{-1}) compared to the other N transformation processes with little variation over time and between stations.

3.6.2. Modeled pore-water profiles and benthic fluxes

The reactive transport model reproduced a good fit for most O_2 and DIN pore-water concentration profiles at the ND station in 2015 (Fig. 4). However, some discrepancies were observed, such as the O_2 and NH_4^+ profiles on August 5th and September 8th, as well as the NO_3^- peak on June 24th. For both studied periods (2015 and 2016), the simulated NH_4^+ and NO_3^- fluxes showed a good fit with the measured fluxes (Fig. 5), with differences still observed within the standard error of the measured values: 4.9, 0.6 and 9.9 μM m^{-2} h^{-1} for NO_3^-, NO_2^- and NH_4^+ fluxes, respectively.

3.6.3. Sensitivity analysis

The sensitivity analysis showed that the OM1 pool input had the largest effect on the magnitude of the NH_4^+ fluxes for each sampling date (Fig. 7). NH_4^+ fluxes increased with the increase in OM1 input and decreased with changes in the proportion of the OM pool, which corresponded to decreased OM1 fluxes by a factor of 3-4. Minor effects on the NH_4^+ fluxes were observed (< 10%) for the other scenarios of change in the environmental factor-related model parameters (Fig. 7). For the NO_3^- fluxes, changes in the bottom water NO_3^- concentrations and the anoxic condition were the main factors influencing flux magnitude and direction (Fig. 8). In April, NO_3^- sediment inward fluxes were increased by increasing the bottom water NO_3^- concentrations and by eliminating O_2 from the bottom water (Figs. 8a, 8b). In June, August and September (Figs. 8c-8f), benthic NO_3^- fluxes reverted from outward to inward when the bottom water O_2 was set to zero and the bottom water NO_3^- concentrations were increased.

4. Discussion

4.1. OM deposition fluxes and diagenetic pathways

Temporal and spatial variations of the benthic dissolved N fluxes in Vilaine Bay (VB) are mainly explained by OM remineralization at the SWI. The model accurately simulated temporal and spatial variations in benthic fluxes by setting high rates of OM decomposition in the upper sediment layer and by essentially varying the input of labile OM (OM1), which constitutes the main fraction (~80%) of the total OM depositional flux. This proportion of OM1 is comparable to that obtained by a modeling study carried out on the Rhone River delta sediments (Pastor et al., 2011; Ait Ballagh et al., 2021), and suggests that most OM inputs into the sediment surface in the VB consists of labile matter. This fraction is characterized in the model by the first-order decomposition rate constant, with this value (16 yr^{-1}) falling within the range of those values (3-33 yr^{-1}) reported in Westrich and Berner (1984) from incubation experiments using fresh planktonic material. The decomposition rate constant of OM2 (0.1 yr^{-1}) lies in the range of those

values reported in the literature (see Paraska et al., 2014; Ait Ballagh et al., 2021), which may correspond to degraded algal cells, containing organic acids and lipids, with a lower degradability than fresh planktonic material (Cowie et al., 1992; Komada et al., 2013). The deposition fluxes of OM1 in this study (275-1,800 μmol cm^{-2} yr^{-1}) are in the range of those reported from anthropogenic impacted estuarine and coastal waters, such as the Aulne and Elorn estuaries (840-3,580 μmol cm^{-2} yr^{-1}; Khalil et al., 2018) , Rhône River delta (260-5,475 μmol cm^{-2} yr^{-1}; Pastor et al., 2011) , and Loch Creran sea (73-1,060 μmol cm^{-2} yr^{-1}; Brigolin et al., 2009). The highest OM1 deposition flux values in the VB (Tables S2) correspond to the maximum Chl *a* contents measured in the sediment surface (Fig. 2), suggesting that this OM has a plant origin (Szymczak-Żyła et al., 2011).

The gradual decrease of O_2 and low O_2 penetration depth suggest rapid O_2 consumption related to OM degradation (Pastor et al., 2011; Rabouille et al., 2021). This is consistent with our model results, which indicate that OM, especially the OM1 pool, was decomposed primarily at the sediment surface using O_2 (Table 1). The difference between the measured and modeled O_2 penetration depth on August 5th and September 8th (Fig. 4a) could not be explained by the limitation of the OM input; if this is the case, the NH_4^+ fluxes would be underestimated by the model. We ascribe this discrepancy to the effects of temperature on microbial metabolism related to the lack of temperature control during the sediment core O_2 profiling in summer, which may have increased O_2 consumption and OM mineralization (Glud et al., 1994; Mogg et al., 2017). In the model, the remaining OM1 and OM2 pool was essentially mineralized through the reduction of SO_4^{2-} (Table 1). This relatively high contribution of SO_4^{2-} reduction, compared to NO_3^- and $Fe(OH)_3$, is in agreement with the high availability of SO_4^{2-} at the upper boundary condition relative to NO_3^- and $Fe(OH)_3$ availability (Canfield, 1993). The contribution to OM decomposition by SO_4^{2-} reduction increases with increasing OM deposition fluxes and particularly when the bottom water O_2 concentration decreases close to the hypoxia level, as was the case at St. B in the summer of 2016. This rapid oxic OM mineralization at the SWI plays a critical role in controlling the bottom water O_2 concentrations as well as benthic nutrient recycling.

4.2. Benthic N transformations: dominance of aerobic processes

The temporal (and spatial) variations in the benthic fluxes and pore-water concentrations of NO_3^- and NO_2^- are consistent with those in the process rates and comparable to those reported in coastal ecosystems subjected to seasonality with regards to the NO_3^- and NO_2^- concentrations in the water column (Jensen et al., 1990; Kemp et al., 1990; Kitidis et al., 2017). The negative concentration gradients of NO_3^- in April 2015, due to large NO_3^- concentrations in the water

column, are in agreement with inward sediment fluxes, which can be attributed to NO_3^- uptake via denitrification (Jorgensen and Sorensen, 1988). These inward sediment NO_3^- fluxes seem proportional to the NO_3^- concentrations in the bottom water. The shift in the NO_3^- flux direction in June 2015 appears to be the result of increasing nitrification, as shown by the NO_3^- concentration peaks in the upper 0.5 cm sediment layer and the bottom water NO_3^- depletion (Jensen et al., 1990), and is in agreement with the measured potential nitrification rates. The temporal and spatial co-variations between the measured potential nitrification and NO_2^- fluxes, as well as the peaks of NO_2^- in the first 1 cm oxic sediment layer, emphasize the role of nitrification in benthic NO_2^- production (Mordy et al., 2010).

Nitrification measurements using the slurry incubation of the first two cm of sediment were taken without limiting O_2 and by adding substrate (NH_4^+). The good fit between the modeled nitrification rates (step 1) and measurements confirms that the conditions were largely aerobic during OM decomposition. The maximum nitrification rates in June suggest that nitrification is dependent on the NH_4^+ produced from OM remineralization (Herbert, 1999). With regards to denitrification, the model-predicted values were much lower than the potential rates measured without limitation of substrate (NO_3^-), implying that denitrification was limited by the availability of NO_3^- (Middelburg et al., 1996; Laverman et al., 2012). Apart from the NO_3^- supply from the water column in April 2015, NO_3^- availability in the sediments was controlled by the nitrification efficiency and therefore by OM remineralization, suggesting that denitrification was closely coupled to nitrification (Risgaard-Petersen, 2003). This also explains the low nitrification/denitrification rate values in August 2015 coinciding with the lowest OM decomposition rates (Tables 1, 2). The low model-predicted DNRA rates are consistent with the potential NO_3^- reduction experiments showing little NH_4^+ production, suggesting that the NO_3^- reduction activity was dominated by denitrification (Laverman et al., 2012). Anammox activity is generally low in eutrophic coastal waters (Bonaglia et al., 2014), which is, in our case, likely related to the low availability of NO_2^- in pore-water (Dalsgaard et al., 2005). These low DNRA values and annamox rates are comparable to the observations made in oxygenated surface sediments from the Gulf of Finland (Jäntti et al., 2011). This dominance of aerobic processes in the benthic N cycle (i.e., coupled nitrification-denitrification), as for aerobic OM mineralization, suggests that the transformation of N in the VB occurs mainly in the uppermost centimeter of the sediments.

4.3. Importance of DON in benthic N cycling

The DON pore-water concentrations in the VB sediments are within the same range as the DIN (mainly NH_4^+) concentrations and are in the same order of magnitude as those reported in the Chesapeake Bay (Burdige and Zheng, 1998) and the St. Lawrence estuary (Alkhatib et al., 2013). The concentration gradients in the DON pore-water profiles were lower than those of NH_4^+ below a depth of 2 cm (Fig. S7), suggesting that DON below this sediment layer may largely consist of refractory compounds slowly producing NH_4^+ in the pore-water (Burdige, 2001; Burdige et al., 2016). The absence of a temporal variation in the DON pore-water profiles indicates that DON cycling in the pore-water, as for NH_4^+ (see below), is relatively independent of seasonal events in the water column, particularly fresh OM inputs from phytoplankton blooms (Hansen and Blackburn, 1992). The positive concentration gradients in the upper 1 cm layer imply DON production and release to the overlying water by diffusion (Alkhatib et al., 2013). However, the weak concentration gradient in the DON pore-water profiles below a depth of 2 cm and much higher DON diffusion time-scales and residence time than those of DIN converge to explain low diffusive DON fluxes (see the Supplementary Material). As observed for NH_4^+ (see below), temporal variations in the diffusive DON fluxes did not reflect large fluctuations in the measured fluxes via incubation.

The benthic DON fluxes measured in the VB represent up to 50% of the dissolved N fluxes (Fig. 5). Although data on benthic DON flux measurements remain scarce in the literature, it appears that their values become truly quantifiable only after the sedimentation of fresh OM (Burdige and Komada, 2002; Eyre and Ferguson, 2002). Parallel temporal and spatial variations in the benthic DON and NH_4^+ fluxes infer that DON was released during OM degradation in the sediment surface. Our measurements confirm those of Hansen and Blackburn (1992), showing that the addition of diatom material to the sediment during laboratory experiments leads to a release of DON to the overlying water, as significant as that of NH_4^+. However, the importance of DON fluxes in benthic N cycling dynamics remains understudied in early diagenetic modeling studies (Paraska et al., 2014). This omission of DON in the RTM is likely related to the uncertainty in estimating its diffusion coefficient (Alperin et al., 1999; Alkhatib et al., 2013), as well as to the scarcity of data concerning benthic DON fluxes and pore-water concentrations (Boynton et al., 2018). Given the significance of DON release in this study, the integration of DON in the RTM may constitute an improvement in order to better estimate the role of this compound in the benthic N budget.

4.4. Phytoplankton-derived OM mineralization at the SWI as the main driver of benthic N fluxes

The benthic NH_4^+ fluxes measured in the VB showed strong temporal and spatial variations, with values lying within the range of those reported in other coastal ecosystems (Boynton et al., 2018). The exchange of NH_4^+ at the SWI can be influenced by several processes, in particular: consumption by benthic primary producers, benthic macrofauna activities, diffusive exchanges between the pore-water and overlying water and direct release from the decomposition of OM that was deposited at the SWI. These processes largely depend on hydrodynamic conditions (water aeration, sediment resuspension, etc.) and OM inputs (production at the SWI and sedimentation).

Primary producers that develop at the SWI (e.g., macroalgae and microphytobenthos) can assimilate NH_4^+ produced in the sediment and affect its exchange between the sediment and overlying water (Sundbäck et al., 2006). In the VB, the presence of macroalgae is limited to the rocky bottom and to the edge and foreshore, both representing less than 10% of the total surface area of the bay (Ehrhold, 2014). Microphytobenthos and particularly benthic diatoms can develop when sufficient light reaches the sediment surface (Miller et al., 1996). The absence of a significant difference between benthic flux measurement values under light and dark conditions in our experiment suggests that microphytobenthos had a minor contribution to the benthic fluxes. The high water column turbidity in the VB (Tessier et al., 2011), which limits microphytobenthos development (Mangan et al., 2020), may explain this hypothesis.

Benthic macrofauna rework sediments, favoring their homogenization and oxygenation, and accelerating the remineralization of sedimentary OM (Shull, 2019). The excretion of dissolved N by benthic macrofauna can also contribute to the enrichment of pore- water and overlying waters with NH_4^+ and DON (Gardner et al., 1993; Yamamuro and Koike, 1998). Among the three main taxa observed in the incubated cores, *Amphiura filiformi*s and *Sternaspis scutata* may favor biodiffusion, whereas *Nucula nitidosa* is instead considered to be a surficial modifier (Queiros et al., 2013). Although the densities of these three species are moderate in the VB (Le Bris and Glémarec, 1996; Ehrhold et al., 2008), they probably enhanced sedimentary OM recycling (Follum and Gray, 1987). The exceptionally high NH_4^+ concentrations in two cores (June 24th and August 5th), found also for phosphate and silicate (Ratmaya, 2018), could be explained by heterogeneities linked to macrofaunal activity. However, no significant correlations between macrofauna density and benthic N transformation rates or N fluxes were found. Additionally, the low bioturbation and bioirrigation coefficients used in the model were sufficient to adjust benthic DIN fluxes, which may indicate the minor influence of benthic macrofaunal activities on benthic N cycling. Although the contribution of benthic macrofauna to benthic dissolved N fluxes could

not be quantified in this study, it probably represents a limited part of the fluxes from the sediment to the water column, but this still needs to be confirmed.

The mineralization of OM in the sediment leads to a build-up of NH_4^+ in the sediment pore-water resulting in the benthic efflux of NH_4^+ (Herbert, 1999; Schulz, 2006). The absence of a significant change in the NH_4^+ pore-water profiles during the temporal study carried out in 2015 agrees with the lack of temporal variations in diffusive NH_4^+ fluxes, implying that a large part of deposited OM is decomposed at the sediment surface before integrating the sediment column, as suggested by Rabouille et al. (2021) for the Louisiana shelf. Relatively low diffusive NH_4^+ fluxes compared to the measured fluxes confirms that significant NH_4^+ production took place through aerobic OM mineralization at the SWI in contact with the bottom water. This pattern is consistent with the relatively low C_{org} values (1.6% DW) of the VB sediments, compared to other eutrophic coastal ecosystems, such as Kiel Bight (3.0-5.0% DW; Balzer et al., 1986) and Aarhus Bay (2.5-3.8% DW; Dale et al., 2008).

In shallow coastal environments, sediment resuspension due to tides, swells and wind may influence benthic fluxes of dissolved substances (Boynton et al., 2018). The absence of a significant difference between benthic flux measurement values during spring and neap tides suggests the minor influence of tidal cycles on SWI DIN and DON exchanges. Sanford et al. (1991) reported that tides had a minor influence on sediment resuspension in the Chesapeake Bay compared to strong wind episodes. In the VB, large sediment resuspension occurs generally in winter in relation with strong hydrodynamic conditions, e.g., during winter storms where several centimeters of sediment can be resuspended (Goubert et al., 2010). This is reflected by the constant depth profiles of granulometry, C_{org} and TN (Bunke et al., 2019). Moreover, sediment resuspension in the VB is often accompanied by high turbidity values in the bottom waters (>100 NTU, Retho et al. 2020). Nevertheless, turbidity values measured at the ND station during the study period remained low (<10 NTU). The persistence of the concentration gradient for the dissolved compounds in the pore-water suggests that sediments have not undergone strong resuspension during the study period. In addition, we did not find any significant correlation between bottom water turbidity and benthic N transformation rates or N fluxes (Table S9).

Different types of OM can be deposited in the VB sediments from external sources. The riverine input of particulate OM is limited due to efficient recycling in the Loire estuary (Relexans et al., 1988) and the presence of a dam in the Vilaine estuary (Traini et al., 2015). Phytoplankton from oceanic waters may not be substantial due to lower biomass than in the VB (Ratmaya et al., 2019). The positive correlation between the measured NH_4^+ fluxes and sediment Chl *a*

concentrations in the VB (Fig. S10a) indicates that benthic NH_4^+ fluxes are dependent on the sedimentation of the phytoplankton (Cowan and Boynton, 1996). This has been shown previously for different coastal ecosystems such as Aarhus Bay (Jensen et al., 1990) and San Francisco Bay (Caffrey, 1995). The observations in the water column and sediment surface, together with the BSi, C_{org} and TN content in the top first five cm of the sediment confirm that diatom blooms are the main source of OM to the VB sediments, with the north-western part as the favored deposition area (Le Bris and Glémarec, 1996; Ehrhold, 2014).

Diatom blooms in the VB are predominantly driven by nutrient inputs associated with floods from the Loire and Vilaine rivers (Figs. 2, S2). After blooms appear, the deposited diatom-derived OM is mostly mineralized aerobically at the SWI within 2-3 weeks and recycled directly to the water column as dissolved inorganic (NH_4^+) and organic N (Fig. 9a). When blooms are absent, benthic dissolved N fluxes decrease and may be supported essentially by a diffusion from the deeper sediment layer, especially for DIN (Fig. 9b). For both situations, the diffusion of DON from a deeper sediment layer is very low, implying that DON is instead gradually mineralized to NH_4^+ in the pore-water. In addition, decomposition of the deposited phytoplanktonic material can rapidly consume O_2 at the sediment surface (within hours to several days) and can be followed by O_2 depletion in the bottom water, especially during summer. This pattern may also be valid for other coastal ecosystems with similar characteristics as the VB, as was reported in oxic sediments from the North Sea (De Borger et al., 2021) and in the seasonally hypoxic sediments of the northern Gulf of Mexico (Rabouille et al., 2021). The overall results lead to conclude that temporal and spatial variations of the benthic DIN and DON fluxes in the VB depend predominantly on the sedimentation of the diatom blooms rather than on the composition of the sediment column itself.

4.5. Ecological implication of benthic DIN fluxes compared to riverine inputs

DIN constitute the limiting nutrient of eutrophication during summer in the VB (Ratmaya et al., 2019). One can wonder how sedimentary and riverine sources contribute to summer DIN budget of the VB. These DIN flux data can be used to give a rough estimate of the role played by sediments in this budget for two different summer scenarios, low water and flood situations in 2015 and 2016 respectively. Benthic DIN fluxes measured in summer 2015 (June-September) at the ND station brings around 225 t N to the VB water column, when extrapolated to the surface of the muddy area (~40% of the total area, 220 km^2, Ehrhold, 2014). For the same period, the Loire delivers around 820 t N by applying a dilution of 20-fold at its outlet, while the Vilaine carried up to 1,120 t N to the VB water column. For this low water scenario, benthic DIN inputs therefore represent around 15% of the riverine inputs. For the summer flood scenario in 2016, benthic DIN

inputs (~360 t N) represent up to 30% of DIN riverine inputs, estimated for 430 t N from the Vilaine and 930 t N from the Loire by applying the same dilution. This higher contribution of benthic DIN source during the summer flood scenario is related to the higher benthic DIN recycling due to higher OM inputs to the sediment surface compared to low water scenario. Despite its uncertainty, this rough estimate suggest that sediments constitute a non-negligible source of DIN to the VB water column, aggravating the effect of riverine DIN inputs. The use of a 3D ecological model (Ménesguen et al., 2019), that takes hydrodynamics into account is required to better estimate the contribution of each DIN source to the VB water column.

5. Conclusion and perspectives

The cross-interpretation of the field observations, laboratory measurements and modeling approach indicate that OM inputs from diatom blooms are the key factor controlling benthic N cycling in the VB. The rapid decomposition of the deposited diatom material at the SWI may be followed by the depletion of the O_2 concentration in the bottom water, especially when blooms occur in summer. Using the same fixed model parameters, the RTM can be used to interpret both the time series and the spatial dataset for the benthic N cycle as a function of the OM deposition rate and the sedimentary environments. The dynamics of the DON fluxes still need to be investigated before they can be integrated into the RTM. The interpolation of benthic DIN flux measurement to the surface area of the VB, suggests that sediments represent a non-negligible source of DIN compared to riverine inputs.

In order to obtain a seasonal and spatial description of the biogeochemical processes in both the sediment and water column, the results presented in this study must be integrated into a 3D ecological model (see Ménesguen et al., 2019 for ECOMARS3D model). Our key results provide the dataset to parameterize the sediment biogeochemical processes (e.g., nutrient transformation, elimination, and/or immobilization) in the ecological model. This integration will improve the ecological model in order to more accurately predict the sequence of river floods, phytoplankton blooms, sedimentation, benthic mineralization and bottom water hypoxia in the VB.

Acknowledgments

This study was funded by The Loire-Brittany Water Agency (AELB). We thank IFREMER-LER/MPL staff, especially the head of the laboratory Nathalie Cochennec-Laureau, Karine Collin, Jean-François Bouget, Michaël Retho, Noémie Delaplanque, Thibault Dinet and Gwenael Bellec for the technical contributions. We would also like to thank the IFREMER

DYNECO/PELAGOS staff: Agnes Youenou, Florian Caradec, Sophie Schmitt, Julien Quéré and Clémence Caule for assistance during the laboratory measurements. We thank Ludovic Helias, Ludovic Boucher, Sébastien Petton for assistance during the field sampling. We thank Philippe Rosa and Anthony Le Bris for the pigment analysis and Lourenço Ribeiro for the taxonomic analysis of the microalgae in the benthic samples. We thank Vincent Soulier, Tifenn Neveu, Valérie Le Cadre, Mathieu Mombrun and Evelyne Goubert for assistance to analyze the sediment physical properties. We thank Sara Mullin for proofreading the English and correcting the English content. The authors acknowledge IFREMER and the Regional Council of the Région des Pays de la Loire for providing funding for the PhD of W. Ratmaya. The authors thank Chen-Tung Arthur Chen for editing the manuscript. Our grateful acknowledgements also go to three anonymous reviewers for their constructive comments and suggestions.

References

Ait Ballagh, F.E., Rabouille, C., Andrieux-Loyer, F., Soetaert, K., Lansard, B., Bombled, B., Monvoisin, G., Elkalay, K., Khalil, K., 2021. Spatial variability of organic matter and phosphorus cycling in Rhône River prodelta sediments (NW Mediterranean Sea, France): a model-data approach. Estuar. Coast. https://dx.doi.org/10.1007/s12237-020-00889-9.

Akbarzadeh, Z., Laverman, A.M., Rezanezhad, F., Raimonet, M., Viollier, E., Shafei, B., Van Cappellen, P., 2018. Benthic nitrite exchanges in the Seine River (France): An early diagenetic modeling analysis. Sci. Total Environ. 628-629, 580-593. https://dx.doi.org/10.1016/j.scitotenv.2018.01.319.

Alkhatib, M., del Giorgio, P.A., Gelinas, Y., Lehmann, M.F., 2013. Benthic fluxes of dissolved organic nitrogen in the lower St. Lawrence estuary and implications for selective organic matter degradation. Biogeosciences 10, 7609-7622. https://dx.doi.org/10.5194/bg-10-7609-2013.

Aller, R.C., Aller, J.Y., 1998. The effect of biogenic irrigation intensity and solute exchange on diagenetic reaction rates in marine sediments. J. Mar. Res. 56, 905-936. https://dx.doi.org/10.1357/002224098321667413.

Alperin, M.J., Martens, C.S., Albert, D.B., Suayah, I.B., Benninger, L.K., Blair, N.E., Jahnke, R.A., 1999. Benthic fluxes and porewater concentration profiles of dissolved organic carbon in sediments from the North Carolina continental slope. Geochim. Cosmochim. Ac. 63, 427-448. https://dx.doi.org/10.1016/s0016-7037(99)00032-0.

Aminot, A., Kérouel, R., 2004. Hydrologie des écosystèmes marins: paramètres et analyses (in French). Éditions Ifremer, Plouzané, France, p. 336.

Aminot, A., Kérouel, R., 2007. Dosage automatique des nutriments dans les eaux marines: méthodes en flux continu (in French). Éditions Ifremer, Plouzané, France, p. 188.

Arndt, S., Jørgensen, B.B., LaRowe, D.E., Middelburg, J.J., Pancost, R.D., Regnier, P., 2013. Quantifying the degradation of organic matter in marine sediments: A review and synthesis. Earth-Sci. Rev. 123, 53-86. https://dx.doi.org/10.1016/j.earscirev.2013.02.008.

Balzer, W., Pollehne, F., Erlenkeuser, H., 1986. Cycling of Organic Carbon in a Coastal Marine System. Springer New York, New York, NY, pp. 325-330. https://dx.doi.org/10.1007/978-1-4612-4932-0_27.

Banta, G.T., Giblin, A.E., Hobbie, J.E., Tucker, J., 1995. Benthic respiration and nitrogen release in Buzzards Bay, Massachusetts. J. Mar. Res. 53, 107-135. https://dx.doi.org/10.1357/0022240953213287.

Belin, C., Soudant, D., Amzil, Z., 2020. Three decades of data on phytoplankton and phycotoxins on the French coast: Lessons from REPHY and REPHYTOX. Harmful Algae 101733. https://dx.doi.org/10.1016/j.hal.2019.101733.

Bianchi, M., Bonin, P., Feliatra, F., 1994. Bacterial nitrification and denitrification rates in the Rhone river plume (northwestern Mediterranean-Sea). Mar. Ecol. Prog. Ser. 103, 197-202. https://dx.doi.org/10.3354/meps103197.

Blackburn, T.H., Henriksen, K., 1983. Nitrogen cycling in different types of sediments from Danish waters[1]. Limnol. Oceanogr. 28, 477-493. https://dx.doi.org/10.4319/lo.1983.28.3.0477.

Bohlen, L., Dale, A.W., Sommer, S., Mosch, T., Hensen, C., Noffke, A., Scholz, F., Wallmann, K., 2011. Benthic nitrogen cycling traversing the Peruvian oxygen minimum zone. Geochim. Cosmochim. Ac. 75, 6094-6111. https://dx.doi.org/10.1016/j.gca.2011.08.010.

Boudreau, B.P., 1997. Diagenetic Models and Their Implementation : Modelling Transport and Reactions in Aquatic Sediments. Springer-Verlag, Berlin.

Boynton, W.R., Ceballos, M.A.C., Bailey, E.M., Hodgkins, C.L.S., Humphrey, J.L., Testa, J.M., 2018. Oxygen and nutrient exchanges at the sediment-water interface: A global synthesis and critique of estuarine and coastal data. Estuar. Coast. 41, 301-333. https://dx.doi.org/10.1007/s12237-017-0275-5.

Brigolin, D., Pastres, R., Nickell, T.D., Cromey, C.J., Aguilera, D.R., Regnier, P., 2009. Modelling the impact of aquaculture on early diagenetic processes in sea loch sediments. Mar. Ecol. Prog. Ser. 388, 63-80. https://dx.doi.org/10.3354/meps08072.

Bunke, D., Leipe, T., Moros, M., Morys, C., Tauber, F., Virtasalo, J.J., Forster, S., Arz, H.W., 2019. Natural and anthropogenic sediment mixing processes in the South-Western Baltic Sea. Front. Mar. Sci. 6, https://dx.doi.org/10.3389/fmars.2019.00677.

Burdige, D.J., 2001. Dissolved organic matter in Chesapeake Bay sediment pore waters. Org. Geochem. 32, 487-505. https://dx.doi.org/10.1016/s0146-6380(00)00191-1.

Burdige, D.J., Alperin, M.J., Homstead, J., Martens, C.S., 1992. The role of benthic fluxes of dissolved organic carbon in oceanic and sedimentary carbon cycling. Geophys. Res. Lett. 19, 1851-1854. https://dx.doi.org/10.1029/92gl02159.

Burdige, D.J., Komada, T., 2002. Sediment Pore Waters In: Hansell, D.A., Carlson, C.A. (Eds.), Biogeochemistry of Marine Dissolved Organic Matter (second edition). Academic Press, San Diego, pp. 535-577. https://dx.doi.org/10.1016/B978-012323841-2/50015-4.

Burdige, D.J., Komada, T., Magen, C., Chanton, J.P., 2016. Modeling studies of dissolved organic matter cycling in Santa Barbara Basin (CA, USA) sediments. Geochim. Cosmochim. Ac. 195, 100-119. https://dx.doi.org/10.1016/j.gca.2016.09.007.

Burdige, D.J., Zheng, S., 1998. The biogeochemical cycling of dissolved organic nitrogen in estuarine sediments. Limnol. Oceanogr. 43, 1796-1813. https://dx.doi.org/10.4319/lo.1998.43.8.1796.

Caffrey, J.M., 1995. Spatial and seasonal patterns in sediment nitrogen remineralization and ammonium concentrations in San Francisco Bay, California. Estuaries 18, 219-233. https://dx.doi.org/10.2307/1352632.

Canavan, R.W., Laverman, A.M., Slomp, C.P., 2007. Modeling nitrogen cycling in a coastal fresh water sediment. Hydrobiologia 584, 27-36. https://dx.doi.org/10.1007/s10750-007-0583-z.

Canavan, R.W., Slomp, C.P., Jourabchi, P., Van Cappellen, P., Laverman, A.M., van den Berg, G.A., 2006. Organic matter mineralization in sediment of a coastal freshwater lake and response to salinization. Geochim. Cosmochim. Ac. 70, 2836-2855. https://dx.doi.org/10.1016/j.gca.2006.03.012.

Canfield, D.E., 1993. Organic Matter Oxidation in Marine Sediments. Springer Berlin Heidelberg, Berlin, Heidelberg, pp. 333-363. https://dx.doi.org/10.1007/978-3-642-76064-8_14.

Carstensen, J., Klais, R., Cloern, J.E., 2015. Phytoplankton blooms in estuarine and coastal waters: Seasonal patterns and key species. Estuar. Coast. Shelf Sci. 162, 98-109. https://dx.doi.org/10.1016/j.ecss.2015.05.005.

Cauwet, G., 1975. Optimisation d'une technique de dosage du carbone organique des sédiments. Chem. Geol. 16, 59-63. https://dx.doi.org/10.1016/0009-2541(75)90091-1.

Chapelle, A., 1991. Modélisation d'un écosystème marin côtier soumis à l'eutrophisation : la Baie de Vilaine (Sud Bretagne). Etude du phytoplancton et du bilan en oxygène (in French). Université Paris VI, p. 214.

Cloern, J.E., 2001. Our evolving conceptual model of the coastal eutrophication problem. Mar. Ecol. Prog. Ser. 210, 223-253. https://dx.doi.org/10.3354/meps210223.

Couture, R.M., Shafei, B., Van Cappellen, P., Tessier, A., Gobeil, C., 2010. Non-steady state modeling of arsenic diagenesis in lake sediments. Environ. Sci. Technol. 44, 197-203. https://dx.doi.org/10.1021/es902077q.

Cowan, J.L.W., Boynton, W.R., 1996. Sediment-water oxygen and nutrient exchanges along the longitudinal axis of Chesapeake Bay: Seasonal patterns, controlling factors and ecological significance. Estuaries 19, 562-580. https://dx.doi.org/10.2307/1352518.

Cowie, G.L., Hedges, J.I., Calvert, S.E., 1992. Sources and relative reactivities of amino acids, neutral sugars, and lignin in an intermittently anoxic marine environment. Geochim. Cosmochim. Ac. 56, 1963-1978. https://dx.doi.org/10.1016/0016-7037(92)90323-b.

Dale, A.W., Aguilera, D.R., Regnier, P., Fossing, H., Knab, N.J., Jørgensen, B.B., 2008. Seasonal dynamics of the depth and rate of anaerobic oxidation of methane in Aarhus Bay (Denmark) sediments. J. Mar. Res. 66, 127-155. https://dx.doi.org/10.1357/002224008784815775.

Dale, A.W., Sommer, S., Bohlen, L., Treude, T., Bertics, V.J., Bange, H.W., Pfannkuche, O., Schorp, T., Mattsdotter, M., Wallmann, K., 2011. Rates and regulation of nitrogen cycling in seasonally hypoxic sediments during winter (Boknis Eck, SW Baltic Sea): Sensitivity to environmental variables. Estuar. Coast. Shelf Sci. 95, 14-28. https://dx.doi.org/10.1016/j.ecss.2011.05.016.

Dalsgaard, T., Nielsen, L.P., Brotas, V., Viaroli, P., Underwood, G., Nedwell, D.B., Sundbäck, K., Rysgaard, S., Miles, A., Bartoli, M., Dong, L., Thornton, D.C.O., Ottosen, L.D.M., Castaldelli, G., Risgaard-Petersen, N., 2000. Protocol handbook for NICE: nitrogen cycling in estuaries: a project under the EU research programme Marine Science and Technology (MAST III). National Environmental Research Institute, Silkeborg, Denmark, p. 64.

Dalsgaard, T., Thamdrup, B., Canfield, D.E., 2005. Anaerobic ammonium oxidation (anammox) in the marine environment. Res. Microbiol. 156, 457-464. https://dx.doi.org/10.1016/j.resmic.2005.01.011.

De Borger, E., Braeckman, U., Soetaert, K., 2021. Rapid organic matter cycling in North Sea sediments. Cont. Shelf Res. 214, 104327. https://dx.doi.org/10.1016/j.csr.2020.104327.

DeMaster, D.J., 1981. The supply and accumulation of silica in the marine environment. Geochim. Cosmochim. Ac. 45, 1715-1732. https://dx.doi.org/10.1016/0016-7037(81)90006-5.

Devol, A.H., 2015. Denitrification, anammox, and N_2 production in marine sediments. Ann. Rev. Mar. Sci. 7, 403-423. https://dx.doi.org/10.1146/annurev-marine-010213-135040.

Ehrhold, A., 2014. Cartes sédimentologiques de Bretagne Sud : Entre baie de Vilaine et archipel de Glénan (in French). QUAE, Versailles, p. 80.

Ehrhold, A., Blanchet, A., Hamon, D., Gaffet, J.-D., Augris, C., Duval, F., 2008. Approche sectorielle subtidale : Identification et caractérisation des habitats benthiques du secteur Vilaine (Réseau de surveillance benthique - Région Bretagne). RST/IFREMER/DYNECO/EB/08-03/REBENT, p. 45. https://archimer.ifremer.fr/doc/00000/2301/.

Eyre, B.D., Ferguson, A.J.P., 2002. Comparison of carbon production and decomposition, benthic nutrient fluxes and denitrification in seagrass, phytoplankton, benthic microalgae- and

macroalgae-dominated warm-temperate Australian lagoons. Mar. Ecol. Prog. Ser. 229, 43-59. https://dx.doi.org/10.3354/meps229043.

Fisher, T.R., Carlson, P.R., Barber, R.T., 1982. Sediment nutrient regeneration in three North Carolina estuaries. Estuar. Coast. Shelf Sci. 14, 101-116. https://dx.doi.org/10.1016/s0302-3524(82)80069-8.

Follum, O.A., Gray, J.S., 1987. Nitrogenous excretion by the sediment-living bivalve Nucula tenuis from the Oslofjord, Norway. Mar. Biol. 96, 355-358. https://dx.doi.org/10.1007/bf00412517.

Gardner, W.S., Briones, E.E., Kaegi, E.C., Rowe, G.T., 1993. Ammonium excretion by benthic invertebrates and sediment-water nitrogen flux in the Gulf of Mexico near the Mississippi River outflow. Estuaries 16, 799. https://dx.doi.org/10.2307/1352438.

Giblin, A.E., Tobias, C.R., Song, B., Weston, N., Banta, G.T., Rivera-Monroy, V.H., 2013. The importance of dissimilatory nitrate reduction to ammonium (DNRA) in the nitrogen cycle of coastal ecosystems. Oceanography 26, 124-131. https://dx.doi.org/10.5670/oceanog.2013.54.

Gilbert, F., Souchu, P., Bianchi, M., Bonin, P., 1997. Influence of shellfish farming activities on nitrification, nitrate reduction to ammonium and denitrification at the water-sediment interface of the Thau lagoon, France. Mar. Ecol. Prog. Ser. 151, 143-153. https://dx.doi.org/10.3354/meps151143.

Glud, R.N., 2008. Oxygen dynamics of marine sediments. Mar. Biol. Res. 4, 243-289. https://dx.doi.org/10.1080/17451000801888726.

Glud, R.N., Gundersen, J.K., Jørgensen, B.B., Revsbech, N.P., Schulz, H.D., 1994. Diffusive and total oxygen uptake of deep-sea sediments in the eastern South Atlantic Ocean: in situ and laboratory measurements. Deep-Sea Res. Pt I 41, 1767-1788. https://dx.doi.org/10.1016/0967-0637(94)90072-8.

Gohin, F., 2011. Annual cycles of chlorophyll-*a*, non-algal suspended particulate matter, and turbidity observed from space and in-situ in coastal waters. Ocean Sci. 7, 705-732. https://dx.doi.org/10.5194/os-7-705-2011.

Goubert, E., Frenod, E., Peeters, P., Thuillier, P., Vested, H.J., Bernard, N., 2010. The use of altimetric data (Altus) in the characterization of hydrodynamic climates controlling hydrosedimentary processes of intertidal mudflat: the Vilaine estuary case (Brittany, France). Revue Paralia 3, 6.17-16.31. https://dx.doi.org/10.5150/revue-paralia.2010.0066.1-6.15.

Gray, J.S., Wu, R.S., Or, Y.Y., 2002. Effects of hypoxia and organic enrichment on the coastal marine environment. Mar. Ecol. Prog. Ser. 238, 249-279. https://dx.doi.org/10.3354/meps238249.

Guillaud, J.-F., Aminot, A., Delmas, D., Gohin, F., Lunven, M., Labry, C., Herbland, A., 2008. Seasonal variation of riverine nutrient inputs in the northern Bay of Biscay (France), and patterns of marine phytoplankton response. J. Marine Syst. 72, 309-319. https://dx.doi.org/10.1016/j.jmarsys.2007.03.010.

Gürevin, C., Erturk, A., Albay, M., 2017. Predicting the effects of sediment based internal nutrient loads on eutrophication in Küçükçekmece Lagoon for rehabilitation planning. Int. J. Sediment Res. 32, 527-554. https://dx.doi.org/10.1016/j.ijsrc.2016.08.002.

Hansen, L.S., Blackburn, T.H., 1992. Effect of algal bloom deposition on sediment respiration and fluxes. Mar. Biol. 112, 147-152. https://dx.doi.org/10.1007/bf00349738.

Hensen, C., Landenberger, H., Zabel, M., Schulz, H.D., 1998. Quantification of diffusive benthic fluxes of nitrate, phosphate, and silicate in the southern Atlantic Ocean. Global Biogeochem. Cy. 12, 193-210. https://dx.doi.org/10.1029/97gb02731.

Herbert, R.A., 1999. Nitrogen cycling in coastal marine ecosystems. FEMS Microbiol. Rev. 23, 563-590. https://dx.doi.org/10.1111/j.1574-6976.1999.tb00414.x.

Hulth, S., Aller, R.C., Canfield, D.E., Dalsgaard, T., Engstrom, P., Gilbert, F., Sundback, K., Thamdrup, B., 2005. Nitrogen removal in marine environments: recent findings and future

research challenges. Mar. Chem. 94, 125-145. https://dx.doi.org/10.1016/j.marchem.2004.07.013.

Ifremer, L.E.R.M.P.d.L., 2015. Qualité du Milieu Marin Littoral - Bulletin de la surveillance 2014. Département du Morbihan (in French). ODE/LITTORAL/LER-MPL/15-06, p. 129. https://archimer.ifremer.fr/doc/00311/42183/.

Jäntti, H., Stange, F., Leskinen, E., Hietanen, S., 2011. Seasonal variation in nitrification and nitrate-reduction pathways in coastal sediments in the Gulf of Finland, Baltic Sea. Aquat. Microb. Ecol. 63, 171-181. https://dx.doi.org/10.3354/ame01492.

Jensen, M.H., Lomstein, E., Sørensen, J., 1990. Benthic NH_4^+ and NO_3^- flux following sedimentation of a spring phytoplankton bloom in Aarhus Bight, Denmark. Mar. Ecol. Prog. Ser. 61, 87-96. https://dx.doi.org/10.3354/meps061087.

Jørgensen, B.B., Revsbech, N.P., 1985. Diffusive boundary layers and the oxygen uptake of sediments and detritus1. Limnol. Oceanogr. 30, 111-122. https://dx.doi.org/10.4319/lo.1985.30.1.0111.

Jorgensen, K.S., Sorensen, J., 1988. Two annual maxima of nitrate reduction and denitrification in estuarine sediment (Norsminde-Fjord, Denmark). Mar. Ecol. Prog. Ser. 48, 147-154. https://dx.doi.org/10.3354/meps048147.

Kemp, W.M., Boynton, W.R., Adolf, J.E., Boesch, D.F., Boicourt, W.C., Brush, G., Cornwell, J.C., Fisher, T.R., Glibert, P.M., Hagy, J.D., Harding, L.W., Houde, E.D., Kimmel, D.G., Miller, W.D., Newell, R.I.E., Roman, M.R., Smith, E.M., Stevenson, J.C., 2005. Eutrophication of Chesapeake Bay: historical trends and ecological interactions. Mar. Ecol. Prog. Ser. 303, 1-29. https://dx.doi.org/10.3354/meps303001.

Kemp, W.M., Sampou, P., Caffrey, J., Mayer, M., Henriksen, K., Boynton, W.R., 1990. Ammonium recycling versus denitrification in Chesapeake Bay sediments. Limnol. Oceanogr. 35, 1545-1563.

Khalil, K., Laverman, A.M., Raimonet, M., Rabouille, C., 2018. Importance of nitrate reduction in benthic carbon mineralization in two eutrophic estuaries: Modeling, observations and laboratory experiments. Mar. Chem. 199, 24-36. https://dx.doi.org/10.1016/j.marchem.2018.01.004.

Kitidis, V., Tait, K., Nunes, J., Brown, I., Woodward, E.M.S., Harris, C., Sabadel, A.J.M., Sivyer, D.B., Silburn, B., Kröger, S., 2017. Seasonal benthic nitrogen cycling in a temperate shelf sea: the Celtic Sea. Biogeochemistry 135, 103-119. https://dx.doi.org/10.1007/s10533-017-0311-3.

Komada, T., Burdige, D.J., Crispo, S.M., Druffel, E.R.M., Griffin, S., Johnson, L., Le, D., 2013. Dissolved organic carbon dynamics in anaerobic sediments of the Santa Monica Basin. Geochim. Cosmochim. Ac. 110, 253-273. https://dx.doi.org/10.1016/j.gca.2013.02.017.

Lansard, B., Rabouille, C., Denis, L., Grenz, C., 2008. In situ oxygen uptake rates by coastal sediments under the influence of the Rhône River (NW Mediterranean Sea). Cont. Shelf Res. 28, 1501-1510. https://dx.doi.org/10.1016/j.csr.2007.10.010.

Laverman, A.M., Pallud, C., Abell, J., Van Cappellen, P., 2012. Comparative survey of potential nitrate and sulfate reduction rates in aquatic sediments. Geochim. Cosmochim. Ac. 77, 474-488. https://dx.doi.org/10.1016/j.gca.2011.10.033.

Laverman, A.M., Van Cappellen, P., van Rotterdam-Los, D., Pallud, C., Abell, J., 2006. Potential rates and pathways of microbial nitrate reduction in coastal sediments. FEMS Microbiol. Ecol. 58, 179-192. https://dx.doi.org/10.1111/j.1574-6941.2006.00155.x.

Lazure, P., Jegou, A.-M., 1998. 3D modelling of seasonal evolution of Loire and Gironde plumes on Biscay Bay continental shelf. Oceanol. Acta 21, 165-177. https://dx.doi.org/10.1016/s0399-1784(98)80006-6.

Le Bris, H., Glémarec, M., 1996. Marine and brackish ecosystems of south Brittany (Lorient and Vilaine Bays) with particular reference to the effect of the turbidity maxima. Estuar. Coast. Shelf Sci. 42, 737-753. https://dx.doi.org/10.1006/ecss.1996.0047.

Le Moal, M., Gascuel-Odoux, C., Menesguen, A., Souchon, Y., Etrillard, C., Levain, A., Moatar, F., Pannard, A., Souchu, P., Lefebvre, A., Pinay, G., 2019. Eutrophication: A new wine in an old bottle? Sci. Total Environ. 651, 1-11. https://dx.doi.org/10.1016/j.scitotenv.2018.09.139.

Lorenzen, C.J., 1967. Determination of chlorophyll and pheo-pigments: spectrophotometric equations. Limnol. Oceanogr. 12, 343-346. https://dx.doi.org/10.2307/2833053.

Mangan, S., Lohrer, A.M., Thrush, S.F., Pilditch, C.A., 2020. Water column turbidity not sediment nutrient enrichment moderates microphytobenthic primary production. J. Mar. Sci. Eng. 8, 732. https://dx.doi.org/10.3390/jmse8100732.

Ménesguen, A., Dussauze, M., Dumas, F., 2018. Designing optimal scenarios of nutrient loading reduction in a WFD/MSFD perspective by using passive tracers in a biogeochemical-3D model of the English Channel/Bay of Biscay area. Ocean Coast. Manage. 163, 37-53. https://dx.doi.org/10.1016/j.ocecoaman.2018.06.005.

Ménesguen, A., Dussauze, M., Dumas, F., Thouvenin, B., Garnier, V., Lecornu, F., Répécaud, M., 2019. Ecological model of the Bay of Biscay and English Channel shelf for environmental status assessment part 1: Nutrients, phytoplankton and oxygen. Ocean Model. 133, 56-78. https://dx.doi.org/10.1016/j.ocemod.2018.11.002.

Middelburg, J.J., Levin, L.A., 2009. Coastal hypoxia and sediment biogeochemistry. Biogeosciences 6, 1273-1293. https://dx.doi.org/10.5194/bg-6-1273-2009.

Middelburg, J.J., Soetaert, K., Herman, P.M.J., Heip, C.H.R., 1996. Denitrification in marine sediments: A model study. Global Biogeochem. Cy. 10, 661-673. https://dx.doi.org/10.1029/96gb02562.

Miller, D.C., Geider, R.J., MacIntyre, H.L., 1996. Microphytobenthos: The ecological role of the "secret garden" of unvegetated, shallow-water marine habitats. Ii. Role in sediment stability and shallow-water food webs. Estuaries 19, 202. https://dx.doi.org/10.2307/1352225.

Mogg, A.O.M., Attard, K.M., Stahl, H., Brand, T., Turnewitsch, R., Sayer, M.D.J., 2017. The influence of coring method on the preservation of sedimentary and biogeochemical features when sampling soft-bottom, shallow coastal environments. Limnol. Oceanogr. Methods 15, 905-915. https://dx.doi.org/10.1002/lom3.10211.

Mordy, C.W., Eisner, L.B., Proctor, P., Stabeno, P., Devol, A.H., Shull, D.H., Napp, J.M., Whitledge, T., 2010. Temporary uncoupling of the marine nitrogen cycle: Accumulation of nitrite on the Bering Sea shelf. Mar. Chem. 121, 157-166. https://dx.doi.org/10.1016/j.marchem.2010.04.004.

Paerl, H.W., 2018. Why does N-limitation persist in the world's marine waters? Mar. Chem. 206, 1-6. https://dx.doi.org/10.1016/j.marchem.2018.09.001.

Paraska, D.W., Hipsey, M.R., Salmon, S.U., 2014. Sediment diagenesis models: Review of approaches, challenges and opportunities. Environ. Modell. Soft. 61, 297-325. https://dx.doi.org/10.1016/j.envsoft.2014.05.011.

Pastor, L., Cathalot, C., Deflandre, B., Viollier, E., Soetaert, K., Meysman, F.J.R., Ulses, C., Metzger, E., Rabouille, C., 2011. Modeling biogeochemical processes in sediments from the Rhône River prodelta area (NW Mediterranean Sea). Biogeosciences 8, 1351-1366. https://dx.doi.org/10.5194/bg-8-1351-2011.

Queiros, A.M., Birchenough, S.N., Bremner, J., Godbold, J.A., Parker, R.E., Romero-Ramirez, A., Reiss, H., Solan, M., Somerfield, P.J., Van Colen, C., Van Hoey, G., Widdicombe, S., 2013. A bioturbation classification of European marine infaunal invertebrates. Ecol. Evol. 3, 3958-3985. https://dx.doi.org/10.1002/ece3.769.

Rabouille, C., Lansard, B., Owings, S.M., Rabalais, N.N., Bombled, B., Metzger, E., Richirt, J., Eitel, E.M., Boever, A.D., Beckler, J.S., Taillefert, M., 2021. Early diagenesis in the hypoxic and acidified zone of the northern Gulf of Mexico: Is organic matter recycling in sediments disconnected from the water column? Front. Mar. Sci. 8, https://dx.doi.org/10.3389/fmars.2021.604330.

1064 Raimbault, P., Pouvesle, W., Diaz, F., Garcia, N., Sempere, R., 1999. Wet-oxidation and
1065 automated colorimetry for simultaneous determination of organic carbon, nitrogen and
1066 phosphorus dissolved in seawater. Mar. Chem. 66, 161-169.
1067 https://dx.doi.org/10.1016/S0304-4203(99)00038-9.
1068 Ratmaya, W., 2018. Rôle des sédiments dans le cycle des nutriments et impacts sur l'eutrophisation
1069 des écosystèmes côtiers (in French). Université de Nantes, p. 212.
1070 Ratmaya, W., Soudant, D., Salmon-Monviola, J., Plus, M., Cochennec-Laureau, N., Goubert, E.,
1071 Andrieux-Loyer, F., Barillé, L., Souchu, P., 2019. Reduced phosphorus loads from the
1072 Loire and Vilaine rivers were accompanied by increasing eutrophication in the Vilaine Bay
1073 (south Brittany, France). Biogeosciences 16, 1361-1380. https://dx.doi.org/10.5194/bg-16-
1074 1361-2019.
1075 Relexans, J.C., Meybeck, M., Billen, G., Brugeaille, M., Etcheber, H., Somville, M., 1988. Algal
1076 and microbial processes involved in particulate organic matter dynamics in the Loire
1077 estuary. Estuar. Coast. Shelf Sci. 27, 625-644. https://dx.doi.org/10.1016/0272-
1078 7714(88)90072-8.
1079 Retho, M., 2019. Etude de la limitation de la biomasse phytoplanctonique par les nutriments dans
1080 le Mor Braz (in French). RST/LER/MPL/19.09, p. 60.
1081 https://archimer.ifremer.fr/doc/00509/62049/.
1082 Retho, M., Quemener, L., Le Gall, C., Repecaud, M., Souchu, P., Gabellec, R., Manach, S., 2020.
1083 MOLIT Vilaine data and metadata from Coriolis Data Centre. SEANOE.
1084 https://dx.doi.org/10.17882/46529.
1085 Risgaard-Petersen, N., 2003. Coupled nitrification-denitrification in autotrophic and heterotrophic
1086 estuarine sediments: On the influence of benthic microalgae. Limnol. Oceanogr. 48, 93-
1087 105. https://dx.doi.org/10.4319/lo.2003.48.1.0093.
1088 Rossignol-Strick, M., 1985. A marine anoxic event on the Brittany Coast, July 1982. J. Coastal
1089 Res. 1, 11-20.
1090 Sanford, L.P., Panageotou, W., Halka, J.P., 1991. Tidal resuspension of sediments in northern
1091 Chesapeake Bay. Mar. Geol. 97, 87-103. https://dx.doi.org/10.1016/0025-3227(91)90020-
1092 5.
1093 Schlitzer, R., 2002. Interactive analysis and visualization of geoscience data with Ocean Data
1094 View. Comput. Geosci. 28, 1211-1218. https://dx.doi.org/10.1016/s0098-3004(02)00040-
1095 7.
1096 Schulz, H.D., 2006. Quantification of Early Diagenesis: Dissolved Constituents in Pore Water and
1097 Signals in the Solid Phase. In: Schulz, H.D., Zabel, M. (Eds.), Marine Geochemistry.
1098 Springer Berlin Heidelberg, Berlin, Heidelberg, pp. 73-124. https://dx.doi.org/10.1007/3-
1099 540-32144-6_3.
1100 Shull, D.H., 2019. Bioturbation☆. In: Cochran, J.K., Bokuniewicz, H.J., Yager, P.L. (Eds.),
1101 Encyclopedia of Ocean Sciences (Third Edition). Academic Press, Oxford, pp. 671-676.
1102 https://dx.doi.org/10.1016/B978-0-12-409548-9.11493-9.
1103 Smetacek, V., 1980. Annual cycle of sedimentation in relation to plankton ecology in western Kiel
1104 Bight. Ophelia 65-76.
1105 Smetacek, V., Zingone, A., 2013. Green and golden seaweed tides on the rise. Nature 504, 84-88.
1106 https://dx.doi.org/10.1038/nature12860.
1107 Soetaert, K., Middelburg, J.J., 2009. Modeling eutrophication and oligotrophication of shallow-
1108 water marine systems: the importance of sediments under stratified and well-mixed
1109 conditions. In: Andersen, J.H., Conley, D.J. (Eds.), Eutrophication in Coastal Ecosystems.
1110 Springer Netherlands, pp. 239-254. https://dx.doi.org/10.1007/978-90-481-3385-7_20.
1111 Sundbäck, K., Miles, A., Linares, F., 2006. Nitrogen dynamics in nontidal littoral sediments: Role
1112 of microphytobenthos and denitrification. Estuar. Coast. 29, 1196-1211.
1113 https://dx.doi.org/10.1007/bf02781820.
1114 Sundbäck, K., Nilsson, P., Nilsson, C., Jönsson, B., 1996. Balance between autotrophic and
1115 heterotrophic components and processes in microbenthic communities of sandy sediments:

A field study. Estuar. Coast. Shelf Sci. 43, 689-706. https://dx.doi.org/10.1006/ecss.1996.0097.

Szymczak-Żyła, M., Kowalewska, G., Louda, J.W., 2011. Chlorophyll-a and derivatives in recent sediments as indicators of productivity and depositional conditions. Mar. Chem. 125, 39-48. https://dx.doi.org/10.1016/j.marchem.2011.02.002.

Taguchi, S., 1982. Sedimentation of newly produced particulate organic matter in a subtropical inlet, Kaneohe Bay, Hawaii. Estuar. Coast. Shelf Sci. 14, 533-544. https://dx.doi.org/10.1016/s0302-3524(82)80075-3.

Tessier, C., Le Hir, P., Dumas, F., Jourdin, F., 2011. Modélisation des turbidités en Bretagne Sud et validation par des mesures in situ. Eur. J. Environ. Civ. En. 12, 179-190. https://dx.doi.org/10.1080/19648189.2008.9693003.

Testa, J.M., Li, Y., Lee, Y.J., Li, M., Brady, D.C., Di Toro, D.M., Kemp, W.M., Fitzpatrick, J.J., 2014. Quantifying the effects of nutrient loading on dissolved O_2 cycling and hypoxia in Chesapeake Bay using a coupled hydrodynamic–biogeochemical model. J. Marine Syst. 139, 139-158. https://dx.doi.org/10.1016/j.jmarsys.2014.05.018.

Thamdrup, B., Dalsgaard, T., 2002. Production of N_2 through anaerobic ammonium oxidation coupled to nitrate reduction in marine sediments. Applied and Environmental Microbiology 68, 1312-1318. https://dx.doi.org/10.1128/aem.68.3.1312-1318.2002.

Torres, E., Couture, R.M., Shafei, B., Nardi, A., Ayora, C., Van Cappellen, P., 2015. Reactive transport modeling of early diagenesis in a reservoir lake affected by acid mine drainage: Trace metals, lake overturn, benthic fluxes and remediation. Chem. Geol. 419, 75-91. https://dx.doi.org/10.1016/j.chemgeo.2015.10.023.

Traini, C., Proust, J.N., Menier, D., Mathew, M.J., 2015. Distinguishing natural evolution and human impact on estuarine morpho-sedimentary development: A case study from the Vilaine Estuary, France. Estuar. Coast. Shelf Sci. 163, 143-155. https://dx.doi.org/10.1016/j.ecss.2015.06.025.

Turner, B.L., Matson, P.A., McCarthy, J.J., Corell, R.W., Christensen, L., Eckley, N., Hovelsrud-Broda, G.K., Kasperson, J.X., Kasperson, R.E., Luers, A., Martello, M.L., Mathiesen, S., Naylor, R., Polsky, C., Pulsipher, A., Schiller, A., Selin, H., Tyler, N., 2003. Illustrating the coupled human-environment system for vulnerability analysis: three case studies. Proc. Natl. Acad. Sci. U S A 100, 8080-8085. https://dx.doi.org/10.1073/pnas.1231334100.

Wang, Y.F., VanCappellen, P., 1996. A multicomponent reactive transport model of early diagenesis: Application to redox cycling in coastal marine sediments. Geochim. Cosmochim. Ac. 60, 2993-3014. https://dx.doi.org/10.1016/0016-7037(96)00140-8.

Ward, B.B., 2008. Nitrification in Marine Systems. In: Capone, D.G., Bronk, D.A., Mulholland, M.R., Carpenter, E.J. (Eds.), Nitrogen in the Marine Environment (2nd Edition). Academic Press, San Diego, pp. 199-261.

Westrich, J.T., Berner, R.A., 1984. The role of sedimentary organic matter in bacterial sulfate reduction: The *G* model tested[1]. Limnol. Oceanogr. 29, 236-249. https://dx.doi.org/10.4319/lo.1984.29.2.0236.

Yamamuro, M., Koike, I., 1998. Concentrations of nitrogen in sandy sediments of a eutrophic estuarine lagoon. Hydrobiologia 386, 37-44. https://dx.doi.org/10.1023/a:1003414028040.

Zhang, J., Gilbert, D., Gooday, A.J., Levin, L., Naqvi, S.W.A., Middelburg, J.J., Scranton, M., Ekau, W., Peña, A., Dewitte, B., Oguz, T., Monteiro, P.M.S., Urban, E., Rabalais, N.N., Ittekkot, V., Kemp, W.M., Ulloa, O., Elmgren, R., Escobar-Briones, E., Van der Plas, A.K., 2010. Natural and human-induced hypoxia and consequences for coastal areas: synthesis and future development. Biogeosciences 7, 1443-1467. https://dx.doi.org/10.5194/bg-7-1443-2010.

Figure captions

Fig. 1 Location of the study area. The off-shore limit of the Vilaine Bay is indicated by a dashed line. The bathymetry (GEBCO bathymetry data in Ocean Data View) is displayed using the colors corresponding to the scale on the right of the graph. The sampling location of the sediment cores is indicated by red circles, the Nord Dumet monitoring station for the temporal study carried out from April to September 2015 and St. A, B, C, & D for the spatial study carried out in July 2016. The green squares correspond to the REPHY monitoring stations. The black dots are the spatial sampling points of the superficial sediments in April 2016.

Fig. 2 Variations in the salinity and river discharge (Loire and Vilaine) (a, e), temperature and dissolved O_2 (b, f), NO_3^- + NO_2^- and NH_4^+ (c, g), Chl *a* in the water column and sediment surface (d, h), at the Nord Dumet monitoring station (St. A) in 2015 (left) and 2016 (right) from January to December. Dashed-dotted horizontal line (panels b & f): hypoxia threshold (63 µM; Middelburg and Levin, 2009; Zhang et al., 2010). Vertical lines: dates of the sediment investigations. ST and NT: spring and neap tides. Color symbols: Chl *a* concentration in the first top cm of the sediment ($n = 3$).

Fig. 3 Depth profiles of the organic carbon, C_{org} (a), total nitrogen, TN (b) and C:N ratios (c) for the triplicate sediment cores at the Nord Dumet monitoring station (St. A) for the temporal study from April to September 2015. No measurements were taken on April 15th.

Fig. 4 Modeled (red curves) and measured (symbols) pore-water concentration profiles of O_2 (a), NH_4^+ (b), NO_3^- (c) and NO_2^- (d) in the temporal study from April to September 2015 conducted at the Nord Dumet monitoring station (St. A). The symbols correspond to the results from the triplicate sediment cores for the nutrients and the O_2 measurements. Dashed lines: sediment-water interface (SWI).

Fig. 5 Measured and simulated NH_4^+ (a), DON (b), NO_3^- (c) and NO_2^- (d) fluxes across the SWI in the Vilaine Bay during the temporal study carried out from April to September 2015 conducted at the Nord Dumet monitoring station (St. A, left) and the spatial study carried out in July 2016 (right). The error bars represent the standard error of the mean ($n = 4$). There were no model simulations for the DON fluxes.

Fig. 6 Relationship between the measured NH_4^+ fluxes and Chl *a* content (a), NH_4^+ and DON fluxes (b) for the temporal study carried out in 2015. The equation and the regression line were obtained from linear regression.

Fig. 7 Model sensitivity analysis showing the response of the benthic NH_4^+ fluxes during the temporal study carried out from April to September 2015 (a-f) to different scenarios of change in environmental factor-related model parameters. The response was calculated as a percentage of change in the NH_4^+ fluxes with regard to the baseline simulation (zero dashed line). The factors lying furthest from the zero dashed line are those causing the greatest change in the NH_4^+ fluxes. Anoxic: zero bottom water O_2 concentrations; BW NO_3^- = 10x [100x]: increase in the bottom water NO_3^- concentrations by 10 fold or 100 fold for August and September; OM1 2x [3x]: increase in the deposition of OM1 by 2 fold (or 3x for August); OM1 <=> OM2: inversing the proportion of OM1 and OM2; k1 OM1 = 2x: increase in the rate constant for the aerobic oxidation of OM1 by 2 fold); k1 OM1 = 1/2 x decrease in the rate constant for the aerobic oxidation of OM1 by one-half; C/N OM1 = 106/16: imposed change in the C/N ratio compared to that in living phytoplankton i.e., Redfield ratio; Db = 10x: increase in the bioturbation coefficient by 10 fold; α = 10x: increase in the bioirrigation coefficient by 10 fold.

Fig. 8 Model sensitivity analysis showing the response of the benthic NO_3^- fluxes during the temporal study carried out from April to September 2015 (a-f) to different scenarios of change in environmental factor-related model parameters. The response was calculated as a percentage of change in the NO_3^- fluxes with regard to the baseline simulation (zero dashed line). The factors lying furthest from the zero dashed line are those causing the greatest change in the NO_3^- fluxes. Anoxic: zero bottom water O_2 concentrations; BW NO_3^- = 10x [100x]: increase in the bottom water NO_3^- concentrations by 10 fold or 100 fold for August and September; OM1 2x [3x]: increase in the deposition of OM1 by 2 fold (or 3x for August); OM1 <=> OM2: inversing the proportion of OM1 and OM2; k1 OM1 = 2x: increase in the rate constant for the aerobic oxidation of OM1 by 2 fold); k1 OM1 = 1/2 x decrease in the rate constant for the aerobic oxidation of OM1 by one-half; C/N OM1 = 106/16: imposed change in the C/N ratio compared to that in living phytoplankton i.e., Redfield ratio; Db = 10x: increase in the bioturbation coefficient by 10 fold; α = 10x: increase in the bioirrigation coefficient by 10 fold.

Fig. 9 Summary diagram of the benthic N fluxes in the Vilaine Bay for two distinct situations: (a) in the presence of a phytoplankton bloom and (b) in the absence of a phytoplankton bloom, based on field observations, laboratory measurements and a modeling study. The terms OM1 and OM2 are used to distinguish between a labile and a less labile pool of organic matter input. DIN and DON stand for dissolved inorganic and organic N, respectively. The different arrow sizes indicate the magnitude of the OM input for each pool, as well as its recycling into DIN (mostly NH_4^+) and DON. The horizontal dashed lines are meant to approximately illustrate the OM turnover time for each pathway (aerobic and anaerobic), estimated from the model rate constants of OM1 and OM2 (Table S3) and the residence time of solutes (Table S6). Where the DON diffusion from pore-water is questioned, this is indicated by a question mark.

Table captions

Table 1 Model-predicted OM decomposition rates through the different pathways for OM1 and OM2 (in parentheses). All values are in µmol C m^{-2} h^{-1}

Table 2 Model-predicted depth-integrated N transformation rates derived from a model simulation. The measured potential nitrification step 1 and NO_3^- reduction rates are indicated in parentheses (mean ± SE). All values are in µmol N m^{-2} h^{-1}.

Fig. 1 Location of the study area. The off-shore limit of the Vilaine Bay is indicated by a dashed line. The bathymetry (GEBCO bathymetry data in Ocean Data View) is displayed using the colors corresponding to the scale on the right of the graph. The sampling location of the sediment cores is indicated by red circles, the Nord Dumet monitoring station for the temporal study carried out from April to September 2015 and St. A, B, C, & D for the spatial study carried out in July 2016. The green squares correspond to the REPHY monitoring stations. The black dots are the spatial sampling points of the superficial sediments in April 2016.

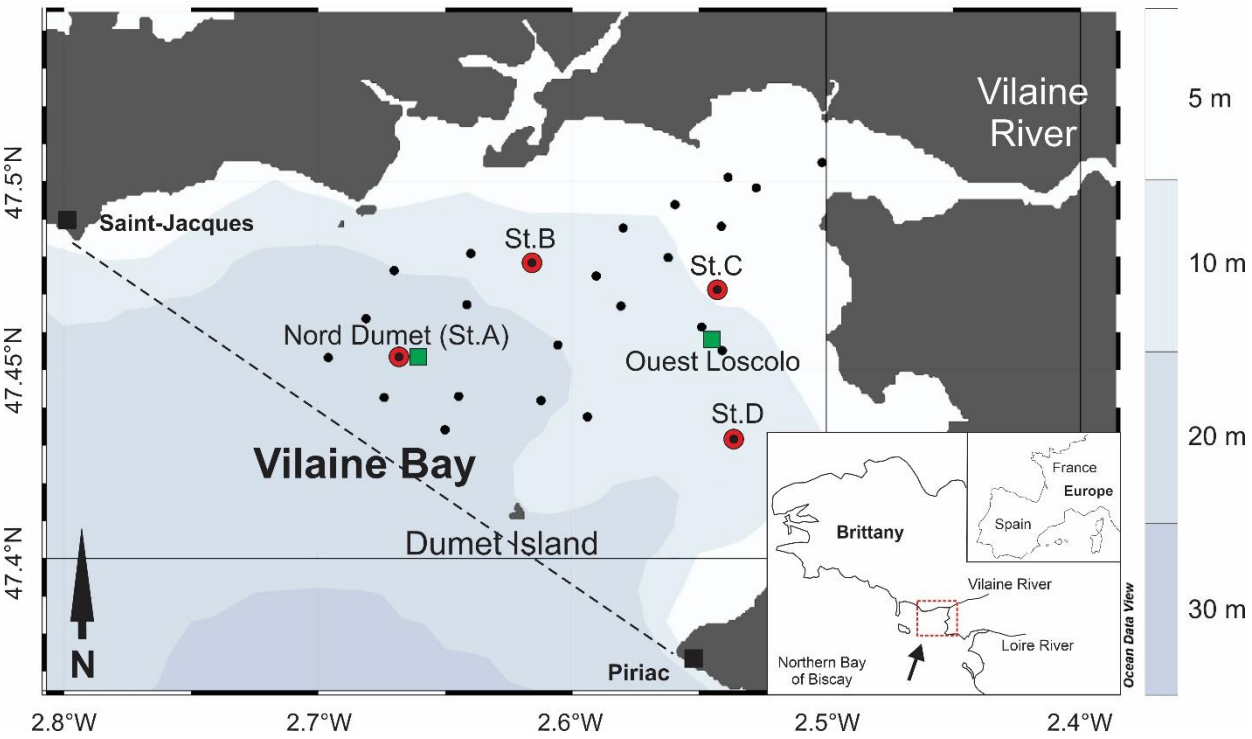

Fig. 2 Variations in the salinity and river discharge (Loire and Vilaine) (a, e), temperature and dissolved O_2 (b, f), $NO_3^- + NO_2^-$ and NH_4^+ (c, g), Chl *a* in the water column and sediment surface (d, h), at the Nord Dumet monitoring station (St. A) in 2015 (left) and 2016 (right) from January to December. Dashed-dotted horizontal line (panels b & f): hypoxia threshold (63 µM; Middelburg and Levin, 2009; Zhang et al., 2010). Vertical lines: dates of the sediment investigations. ST and NT: spring and neap tides. Color symbols: Chl *a* concentration in the first top cm of the sediment ($n = 3$).

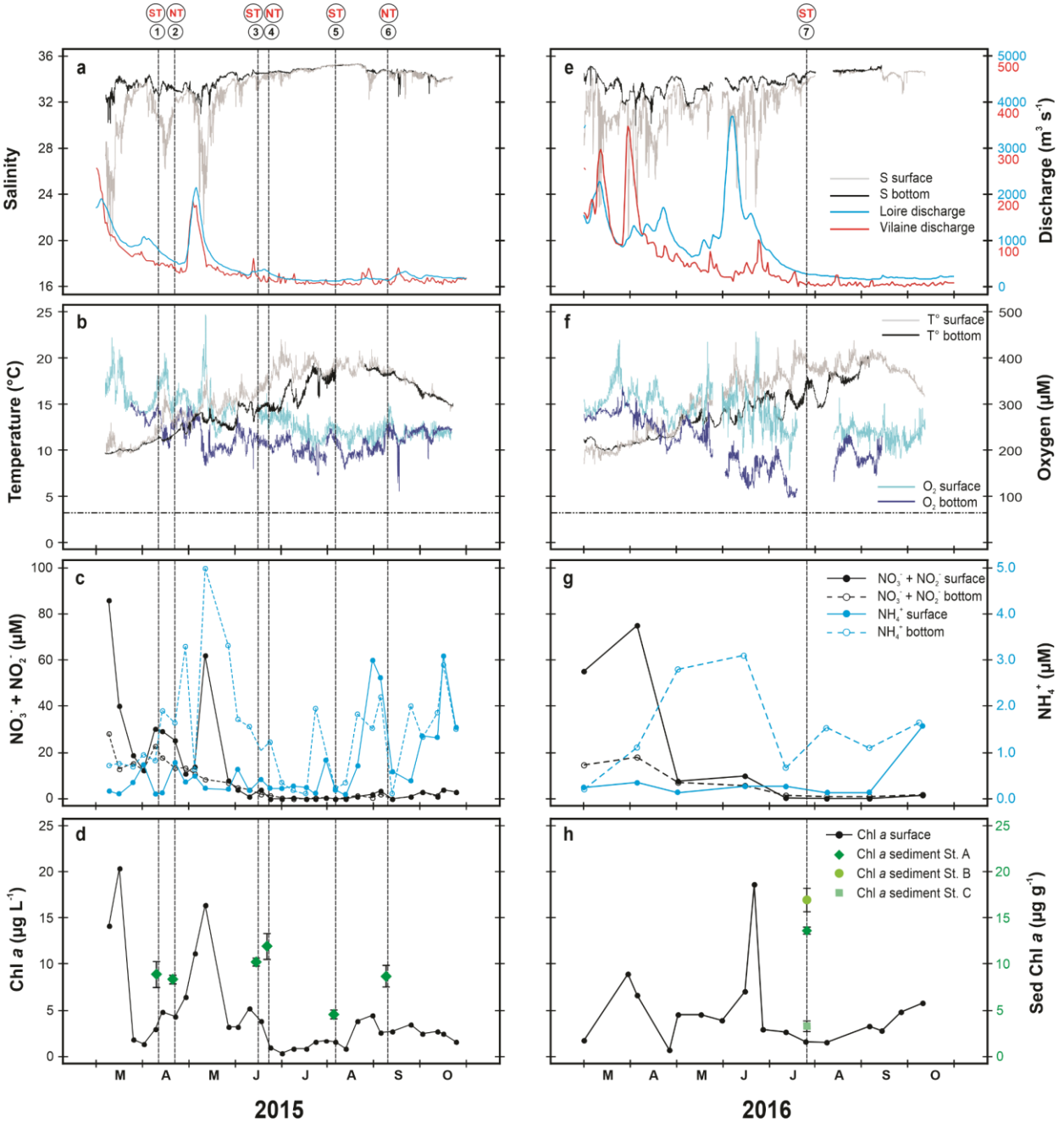

Fig. 3 Depth profiles of the organic carbon, C_{org} (a), total nitrogen, TN (b) and C:N ratios (c) for the triplicate sediment cores at the Nord Dumet monitoring station (St. A) for the temporal study from April to September 2015. No measurements were taken on April 15th.

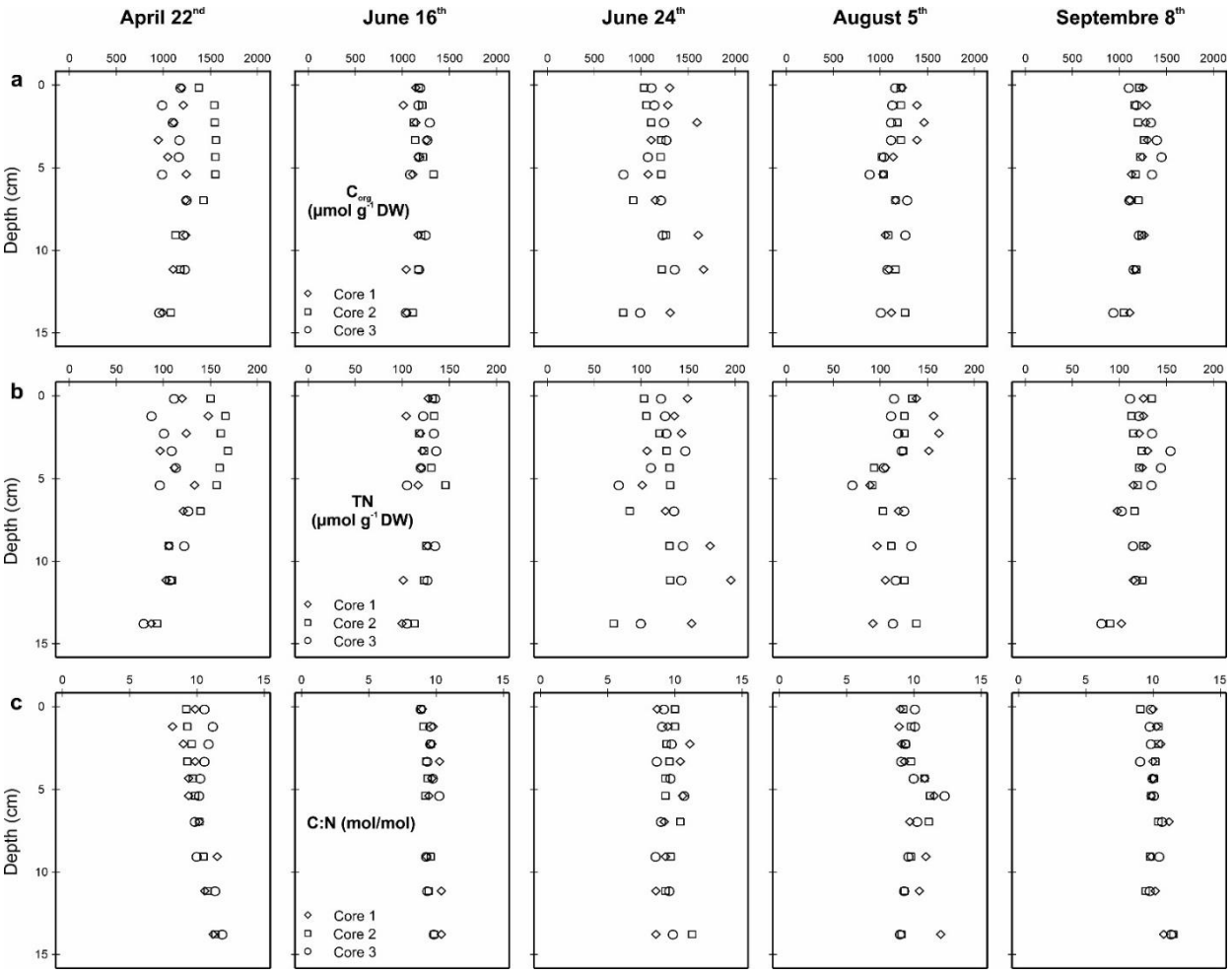

Fig. 4 Modeled (red curves) and measured (symbols) pore-water concentration profiles of O_2 (a), NH_4^+ (b), NO_3^- (c) and NO_2^- (d) in the temporal study from April to September 2015 conducted at the Nord Dumet monitoring station (St. A). The symbols correspond to the results from the triplicate sediment cores for the nutrients and the O_2 measurements. Dashed lines: sediment-water interface (SWI).

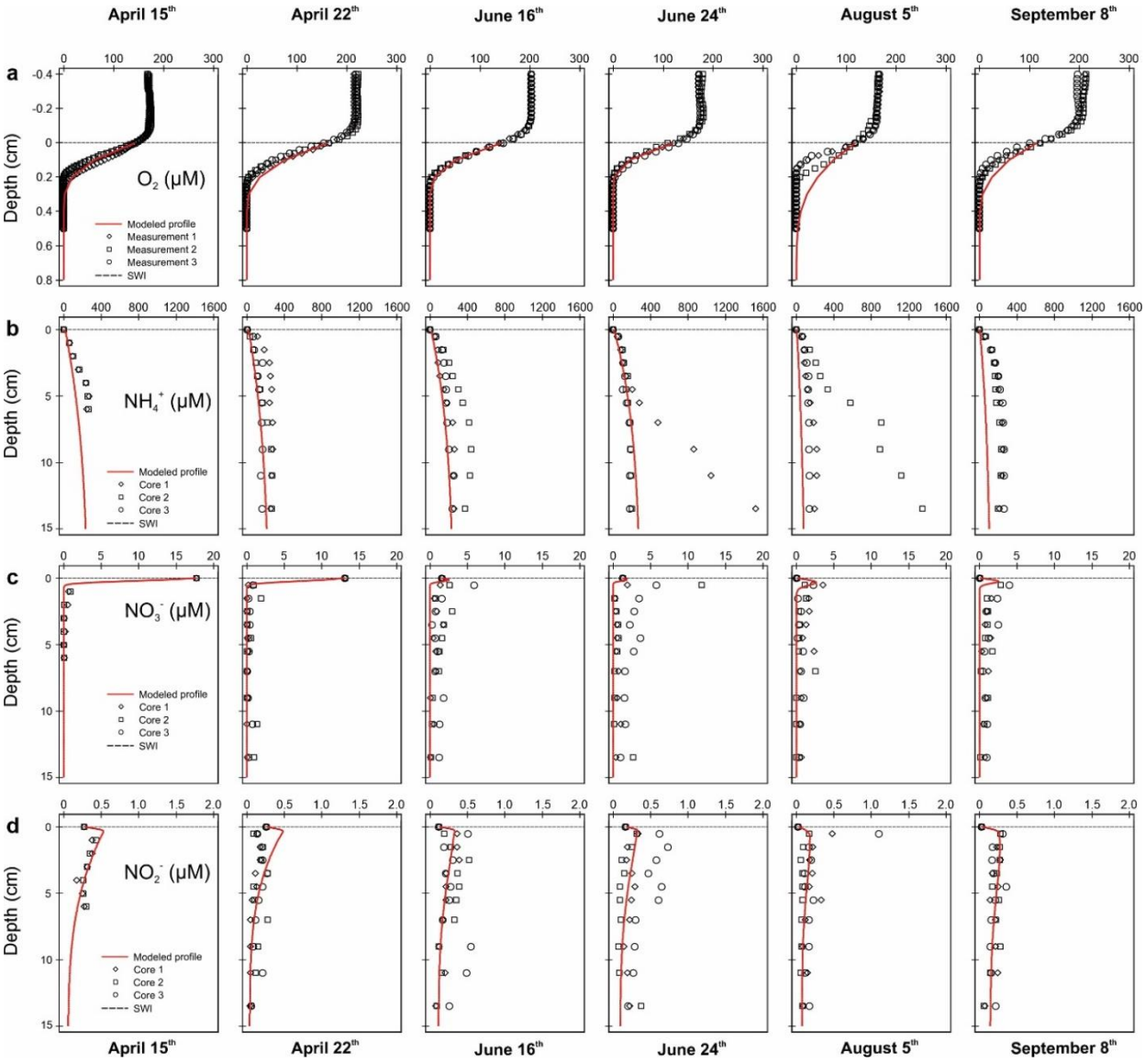

Fig. 5 Measured and simulated NH_4^+ (a), DON (b), NO_3^- (c) and NO_2^- (d) fluxes across the SWI in the Vilaine Bay during the temporal study carried out from April to September 2015 conducted at the Nord Dumet monitoring station (St. A, left) and the spatial study carried out in July 2016 (right). The error bars represent the standard error of the mean (*n = 4*). There were no model simulations for the DON fluxes.

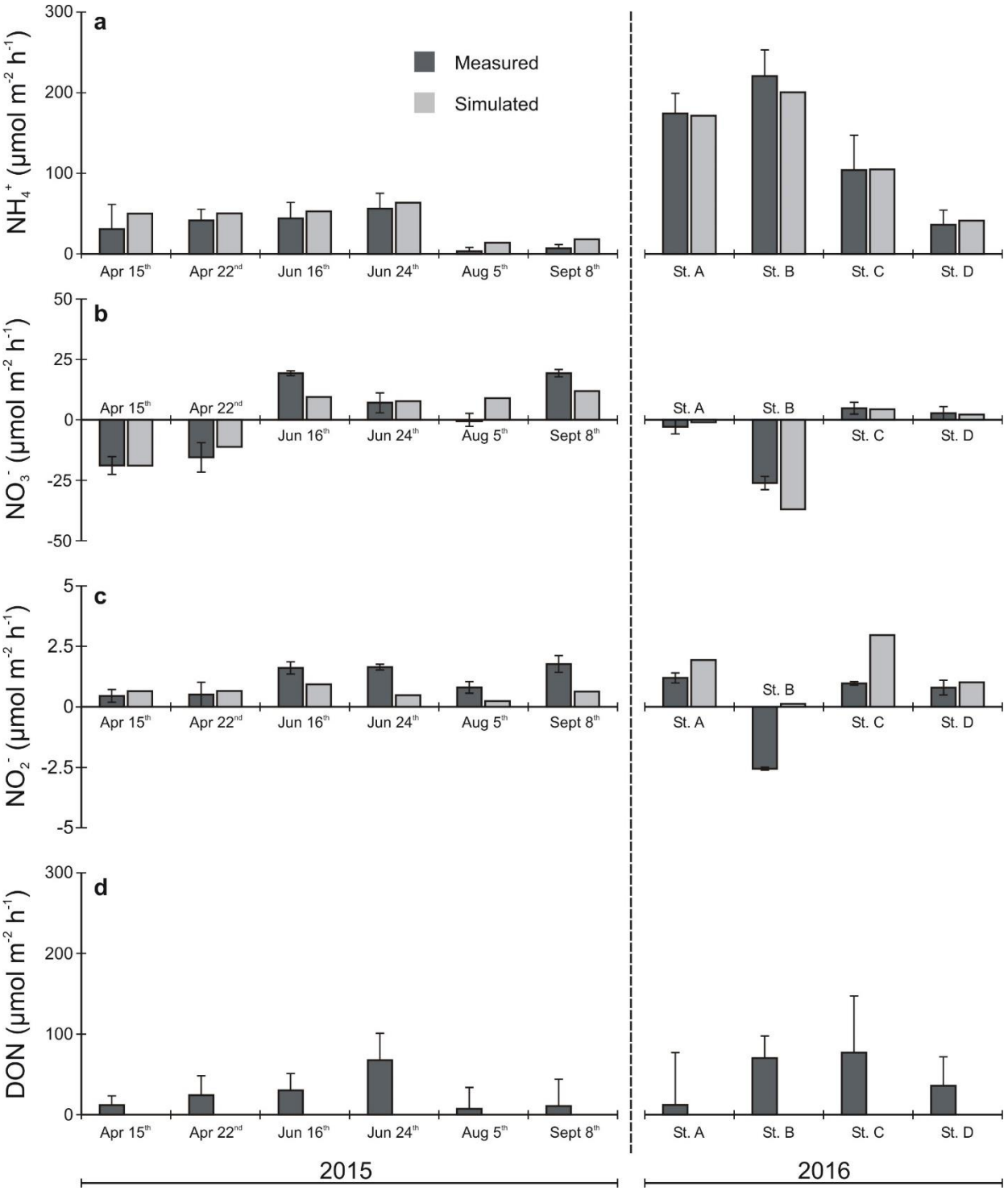

Fig. 6 Relationship between the measured NH_4^+ fluxes and Chl *a* content (a), NH_4^+ and DON fluxes (b) for the temporal study carried out in 2015. The equation and the regression line were obtained from linear regression.

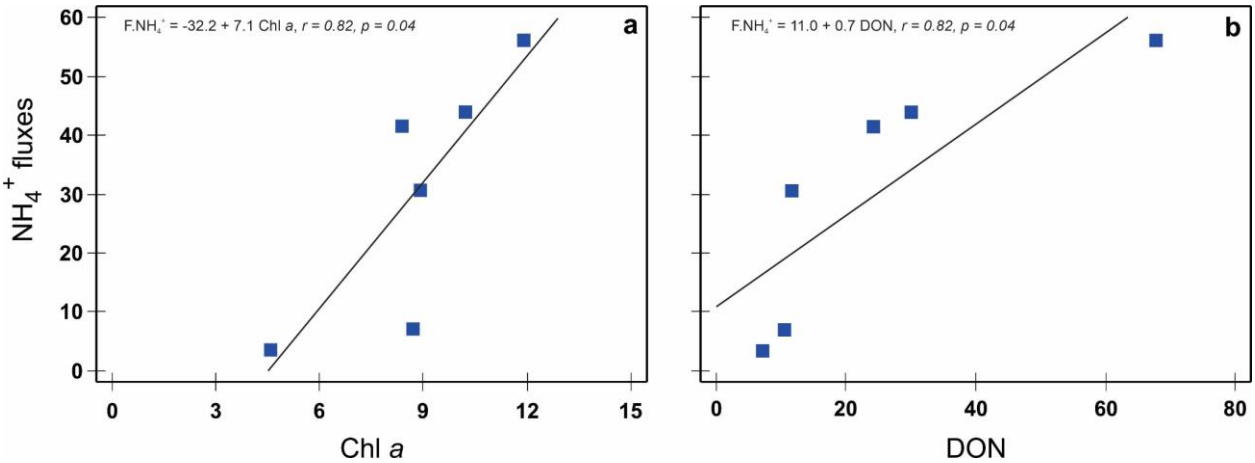

Fig. 7 Model sensitivity analysis showing the response of the benthic NH_4^+ fluxes during the temporal study carried out from April to September 2015 (a-f) to different scenarios of change in environmental factor-related model parameters. The response was calculated as a percentage of change in the NH_4^+ fluxes with regard to the baseline simulation (zero dashed line). The factors lying furthest from the zero dashed line are those causing the greatest change in the NH_4^+ fluxes. Anoxic: zero bottom water O_2 concentrations; BW NO_3^- = 10x [100x]: increase in the bottom water NO_3^- concentrations by 10 fold or 100 fold for August and September; OM1 2x [3x]: increase in the deposition of OM1 by 2 fold (or 3x for August); OM1 <=> OM2: inversing the proportion of OM1 and OM2; k1 OM1 = 2x: increase in the rate constant for the aerobic oxidation of OM1 by 2 fold); k1 OM1 = 1/2 x decrease in the rate constant for the aerobic oxidation of OM1 by one-half; C/N OM1 = 106/16: imposed change in the C/N ratio compared to that in living phytoplankton i.e., Redfield ratio; Db = 10x: increase in the bioturbation coefficient by 10 fold; α = 10x: increase in the bioirrigation coefficient by 10 fold.

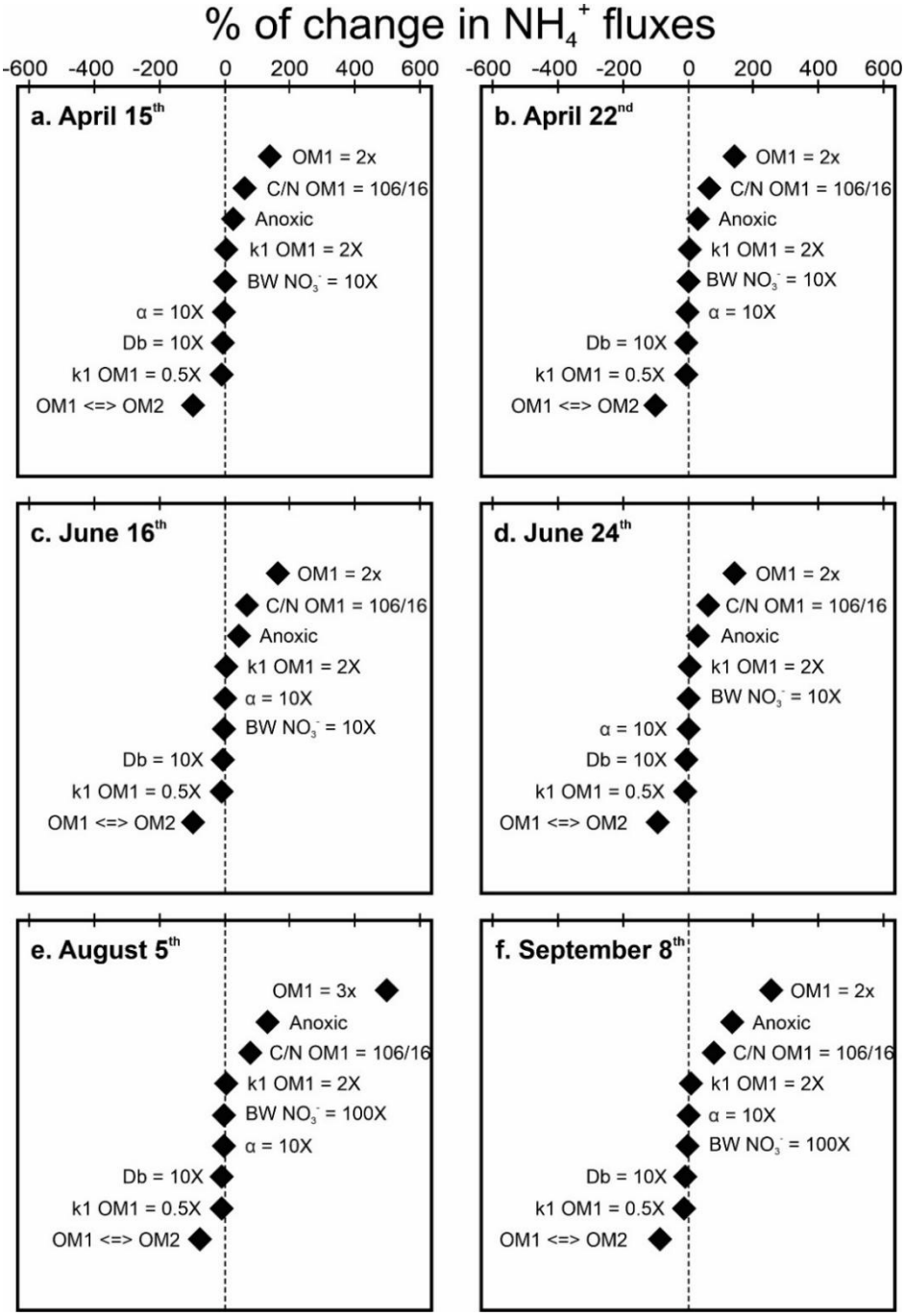

Fig. 8 Model sensitivity analysis showing the response of the benthic NO_3^- fluxes during the temporal study carried out from April to September 2015 (a-f) to different scenarios of change in environmental factor-related model parameters. The response was calculated as a percentage of change in the NO_3^- fluxes with regard to the baseline simulation (zero dashed line). The factors lying furthest from the zero dashed line are those causing the greatest change in the NO_3^- fluxes. Anoxic: zero bottom water O_2 concentrations; BW NO_3^- = 10x [100x]: increase in the bottom water NO_3^- concentrations by 10 fold or 100 fold for August and September; OM1 2x [3x]: increase in the deposition of OM1 by 2 fold (or 3x for August); OM1 <=> OM2: inversing the proportion of OM1 and OM2; k1 OM1 = 2x: increase in the rate constant for the aerobic oxidation of OM1 by 2 fold); k1 OM1 = 1/2 x decrease in the rate constant for the aerobic oxidation of OM1 by one-half; C/N OM1 = 106/16: imposed change in the C/N ratio compared to that in living phytoplankton i.e., Redfield ratio; Db = 10x: increase in the bioturbation coefficient by 10 fold; α = 10x: increase in the bioirrigation coefficient by 10 fold.

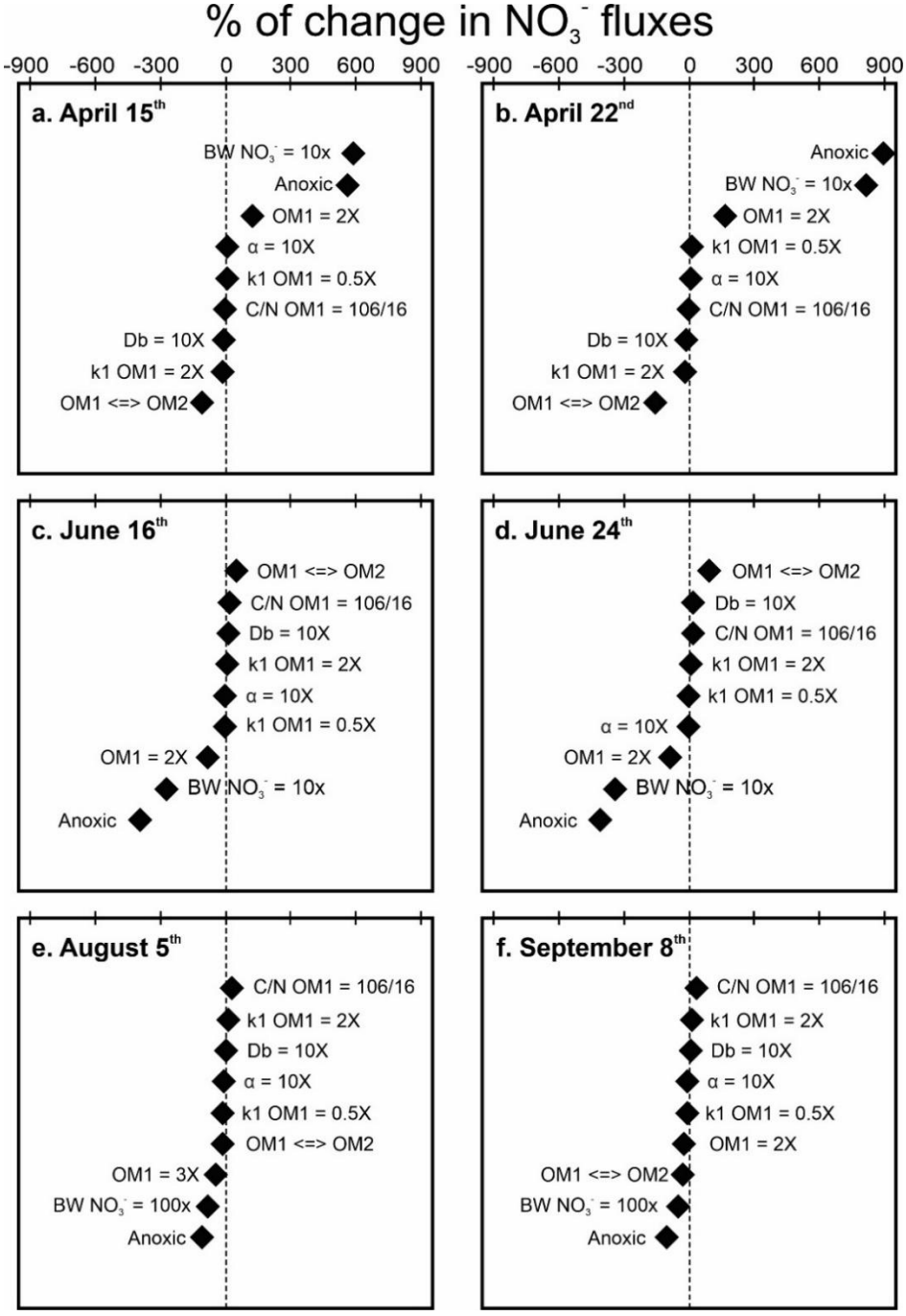

Fig. 9 Summary diagram of the benthic N fluxes in the Vilaine Bay for two distinct situations: (a) in the presence of a phytoplankton bloom and (b) in the absence of a phytoplankton bloom, based on field observations, laboratory measurements and a modeling study. The terms OM1 and OM2 are used to distinguish between a labile and a less labile pool of organic matter input. DIN and DON stand for dissolved inorganic and organic N, respectively. The different arrow sizes indicate the magnitude of the OM input for each pool, as well as its recycling into DIN (mostly NH_4^+) and DON. The horizontal dashed lines are meant to approximately illustrate the OM turnover time for each pathway (aerobic and anaerobic), estimated from the model rate constants of OM1 and OM2 (Table S3) and the residence time of solutes (Table S6). Where the DON diffusion from pore-water is questioned, this is indicated by a question mark.

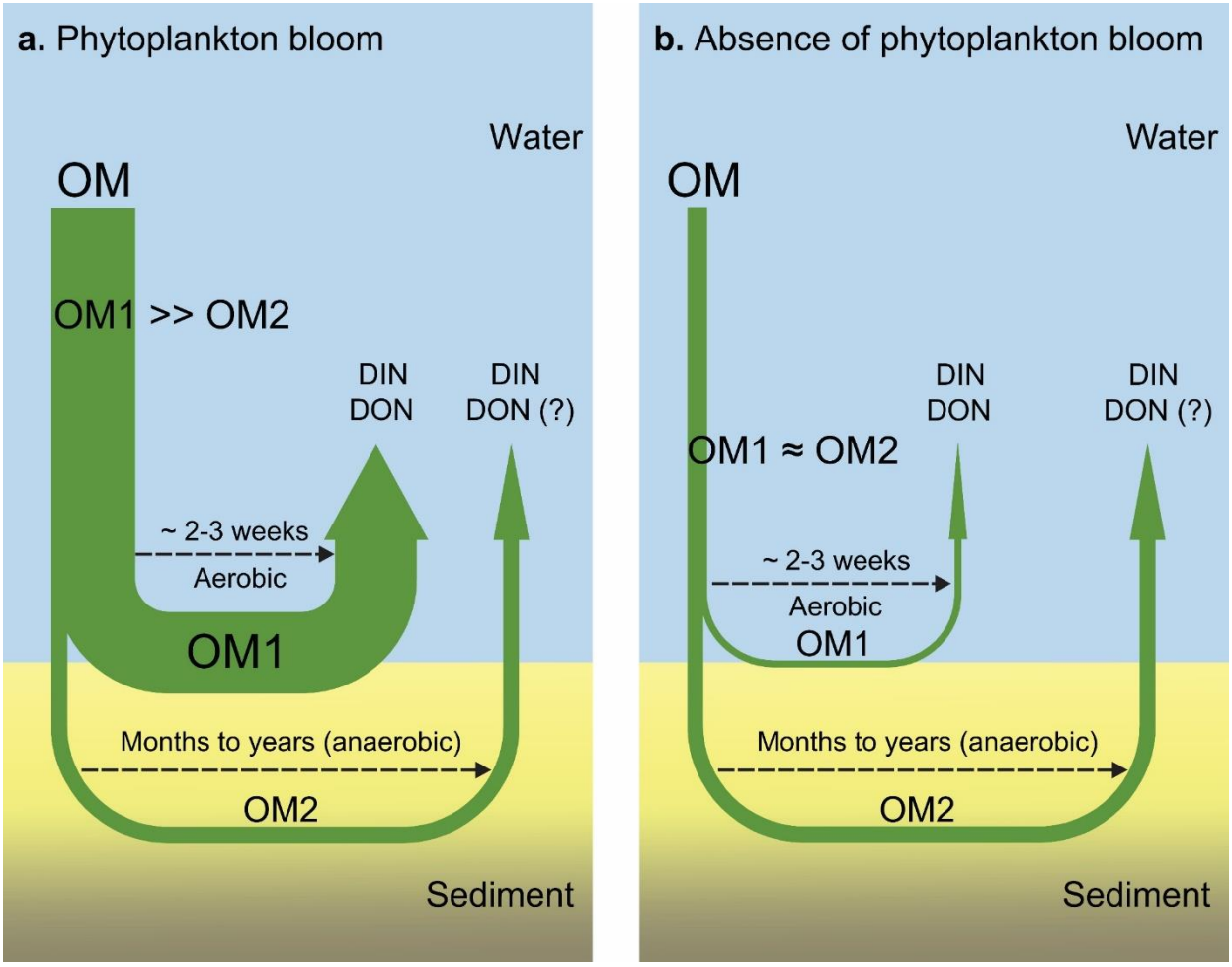

Table 1 Model-predicted OM decomposition rates through the different pathways for OM1 and OM2 (in parentheses). All values are in µmol C m^{-2} h^{-1}

Processes	April 15th	April 22nd	June 16th	June 24th	August 5th	September 8th	St. A	St. B	St. C	St. D
O_2	475.8 (3.9)	506.4 (4.9)	605.8 (5.9)	629.7 (5.3)	261.3 (9.1)	343.3 (6.7)	1,307.9 (9.3)	1,164.4 (3.9)	862.6 (9.3)	298.9 (3.1)
NO_3^- [a]	45.5 (1.1)	36.5 (1.0)	23.1 (0.7)	19.7 (0.5)	12.9 (1.6)	17.8 (1.1)	2.6 (0.1)	49.0 (0.5)	4.6 (0.1)	4.1 (0.1)
$Fe(OH)_3$	21.3 (1.5)	21.6 (1.8)	20.9 (1.7)	20.7 (1.4)	18.1 (6.7)	19.7 (3.5)	21.1 (1.2)	20.9 (0.6)	20.7 (1.8)	23.1 (2.0)
SO_4^{2-}	111.5 (23.8)	98.7 (26.8)	133.5 (40.4)	168.5 (44.8)	19.0 (30.5)	43.0 (32.4)	354.1 (82.4)	723.1 (69.0)	238.5 (85.0)	120.0 (39.7)
Total [b]	654.1 (30.5)	663.2 (34.7)	783.3 (48.7)	838.6 (52.2)	311.3 (48.1)	423.7 (43.9)	1,685.8 (93.0)	1,957.5 (73.9)	1,126.4 (96.3)	446.2 (44.9)

[a] Sum of the denitrification and DNRA rates (see section 2.4.2. and Table S1).
[b] Total rates of all OM decomposition pathways.

Table 2 Model-predicted depth-integrated N transformation rates derived from a model simulation. The measured potential nitrification step 1 and NO_3^- reduction rates are indicated in parentheses (mean ± SE). All values are in µmol N m^{-2} h^{-1}.

Processes	April 15th	April 22nd	June 16th	June 24th	August 5th	September 8th	St. A	St. B	St. C	St. D
Nitrification 1	18.4 (11.5 ± 0.4)	19.1 (16.7 ± 0.6)	29.2 (20.0 ± 1.6)	24.2 (28.0 ± 2.9)	20.8 (14.0 ± 2.5)	27.5 (12.0 ± 1.3)	3.1 (7.3 ± 0.7)	0.4 (0.0 ± 0.0)	7.3 (2.8 ± 0.6)	6.6 (2.2 ± 0.7)
Nitrification 2	17.7	18.3	28.2	23.7	20.5	26.8	1.1	2.0	5.4	5.5
Denitrification	35.5 (52.4 ± 6.6)	28.6 (60.7 ± 8.8)	18.1 (73.6 ± 8.2)	15.4 (119.0 ± 24.8)	11.2 (na)	14.5 (na)	2.0 (na)	37.6 (na)	3.6 (na)	3.2 (na)
DNRA	1.17	0.94	0.60	0.51	0.37	0.48	0.07	1.24	0.12	0.11
Anammox	0.08	0.10	0.06	0.06	0.08	0.07	0.04	0.06	0.03	0.05

Supplementary materials

Temporal and spatial variations in benthic nitrogen cycling in a temperate macro-tidal coastal ecosystem: observation and modeling

Widya Ratmaya*[1], Anniet M. Laverman[2], Christophe Rabouille[3], Zahra Akbarzadeh[4], Françoise Andrieux-Loyer[5], Laurent Barillé[6], Anne-Laure Barillé[7], Yoann Le Merrer[1], Philippe Souchu[1]

[1] Ifremer – LER MPL, Rue de l'Ile d'Yeu, BP 21105, 44311 Nantes Cedex 03, France

[2] Université de Rennes, CNRS, UMR 6553 ECOBIO, Campus Beaulieu, 263 avenue du Général Leclerc, Rennes F-35042, France

[3] Laboratoire des Sciences du Climat et de l'Environnement, CEA-CNRS UNMR 1572, Av. de la Terrasse, 91198 Gif sur Yvette, France

[4] Ecohydrology Research Group, Water Institute and Department of Earth and Environmental Sciences, University of Waterloo, 200 University Avenue West, Waterloo, Ontario, Canada

[5] Ifremer – DYNECO PELAGOS, ZI Pointe du Diable, 29280 Plouzané, France

[6] Université de Nantes, Mer Molécules Santé EA 2160, Faculté des Sciences et des Techniques, BP 92208, 44322 Nantes cedex 3, France

[7] Bio-Littoral, Immeuble Le Nevada, 2 Rue du Château de l'Eraudière CS 80693, 44306 Nantes

* Email: widyaratmaya@gmail.com

Laboratoire Environnement Ressource Morbihan – Pays de la Loire, Centre Ifremer de Nantes, Rue de l'Ile d'Yeu, BP 21105, 44311 Nantes Cedex 03, France.

Table S1 Reaction network and rate formulation used in the model.

Description	Reaction formulation[a]	Rate expression[b, c]
Aerobic respiration	$OM + xO_2 + (2z-y)HCO_3^- \rightarrow yNH_4^+ + zHPO_4^{2-} + (x-y+2z)CO_2 + (x-y+2z)H_2O$	$R1 = k1\,[OM] \cdot \frac{[O_2]}{[O_2] + kO} \cdot F_T$
Denitrification	$OM + 0.8xNO_3^- \rightarrow 0.4xN_2 + yNH_4^+ + 0.8xNO_2^- + zHPO_4^{2-} + (0.8x+y-2z)HCO_3^- + (0.2x-y+2z)CO_2 + (0.6x-y+2z)H_2O$	$R2 = k2\,[OM] \cdot \frac{[NO_3^-]}{[NO_3^-] + kNO} \cdot \frac{kinO}{[O_2] + kinO} \cdot 1 - F_{DNRA} \cdot F_T$
DNRA	$OM + 0.5xNO_3^- \rightarrow (0.5x+y)NH_4^+ + (0.5xNO_2^-) + zHPO_4^{2-} + (y-2z)HCO_3^- + (x-y+2z)CO_2 + (0.5x-y+2z)H_2O$	$R3 = k2\,[OM] \cdot \frac{[NO_3^-]}{[NO_3^-] + kNO} \cdot \frac{kinO}{[O_2] + kinO} \cdot F_{DNRA} \cdot F_T$
Nitrification step 1	$NH_4^+ + 1.5O_2 \rightarrow NO_2^- + H_2O$	$R4 = k_{nit1} \cdot \frac{[NH_4^+]}{[NH_4^+] + kmNH4ao} \cdot \frac{[O_2]}{[O_2] + kmO2ao} \cdot F_T$
Nitrification step 2	$NO_2^- + 0.5O_2 \rightarrow NO_3^-$	$R5 = k_{nit2} \cdot \frac{[NO_2^-]}{[NO_2^-] + khNIT} \cdot \frac{[O_2]}{[O_2] + khO} \cdot F_T$
Anammox	$NH_4^+ + NO_2^- \rightarrow N_2 + 2H_2O$	$R6 = k_{anx} \cdot \frac{[NH_4^+]}{[NH_4^+] + khNH4} \cdot \frac{[NO_2^-]}{[NO_2^-] + khNO} \cdot \frac{kinO}{[O_2] + kinO} \cdot F_T$

[a] $OM = x(CH_2O)_{org} + y(NH_3)_{org} + z(H_3PO_4)_{org}$, where x, y, z represent the CNP ratios,

[b] F_{DNRA} = fraction of the total nitrate reduction occurring via DNRA (5%),

[c] F_T = temperature correction for the rates. $F_T = \frac{K_1 \cdot exp(\gamma_1 \cdot (T - T_1))}{1 + K_1 \cdot exp(\gamma_1 \cdot (T - T_1) - K_1} \cdot \frac{K_2 \cdot exp(\gamma_2 \cdot (T_2 - T))}{1 + K_2 \cdot exp(\gamma_2 \cdot (T_2 - T) - K_2}$, where T_1 and T_2 are the lower and upper temperature for the OM decay, respectively; K_1 and K_2 are the coefficient rates for the lower and upper temperature, respectively; γ_1 and γ_2 are the temperature rate multipliers for T_1 and T_2, respectively (see Cole and Wells, 2006 for details).

Table S2 Boundary conditions used in the model.

Parameters	Apr 15th	Apr 22nd	Jun 16th	Jun 24th	Aug 5th	Sep 8th	St. A	St. B	St. C	St. D	Unit	Sources
	2015 (Nord Dumet monitoring station/St. A)						2016					
Solutes												
O_2	142 (84%)	161 (95%)	142 (82%)	120 (75%)	118 (93%)	114 (101%)	198 (80%)	96 (37%)	170 (70%)	198 (79%)	µM	I
NO_3^-	17.7	13.1	1.60	1.30	0.07	0.04	0.37	6.82	0.20	0.47	µM	I
NO_2^-	0.27	0.26	0.12	0.17	0.03	0.03	0.04	0.73	0.00	0.06	µM	I
NH_4^+	1.90	3.30	1.03	1.23	0.21	0.09	0.80	4.40	1.80	1.61	µM	I
Fe^{2+}	0	0	0	0	0	0	0	0	0	0	µM	I
SO_4^{2-} [a]	28	28	28	28	28	28	28	28	28	28	mM	M
Solids												
OM1	600	600	700	750	275	375	1,500	1,800	1,000	400	µmol C cm^{-2} yr^{-1}	M
OM2	150	150	170	180	120	120	300	300	300	150	µmol C cm^{-2} yr^{-1}	M
$Fe(OH)_3$	75	75	75	75	75	75	75	75	75	75	µmol cm^{-2} yr^{-1}	M

Solute concentrations were obtained from the measurements. Solid fluxes were constrained from the model fitting (see Methods). [a] The SO_4^{2-} concentration was constrained from the measured salinity. Sources: **M**, constrained by the model fitting; **I**, independently determined from the field data.

Table S3 Reaction parameter values used in the model.

Parameters	Apr 15th	Apr 22nd	Jun 16th	Jun 24th	Aug 5th	Sep 8th	St. A	St. B	St. C	St. D	Unit	Source	Ref.	Description
	2015 (Nord Dumet monitoring station/St. A)						2016							
Fixed														
C:N OM1	10	10	10	10	10	10	10	10	10	10		M		C:N ratio for OM1
C:N OM2	15	15	15	15	15	15	15	15	15	15		M		C:N ratio for OM2
k_O	5	5	5	5	5	5	5	5	5	5	µM	L	2, 4, 5	Limitation of O_2 for aerobic oxidation
k_{NO}	5	5	5	5	5	5	5	5	5	5	µM	L	2, 4, 5	Limitation of NO_3^- for denitrification
k_{mNH4ao}	5	5	5	5	5	5	5	5	5	5	µM	L	1	Limitation of NH_4^+ for nitrification step 1
k_{mO2ao}	5	5	5	5	5	5	5	5	5	5	µM	L	1	Limitation of O_2 for nitrification step 1
k_{hNIT}	1	1	1	1	1	1	1	1	1	1	µM	L	1	Limitation of NO_2^- for nitrification step 2
k_{HO}	5	5	5	5	5	5	5	5	5	5	µM	L	1	Limitation of O_2 for nitrification step 2
k_{hno}	1	1	1	1	1	1	1	1	1	1	µM	L	3	Limitation of NO_2^- for anammox
k_{hnh}	1	1	1	1	1	1	1	1	1	1	µM	L	3	Limitation of NH_4^+ for anammox
k_{inO}	6	6	6	6	6	6	6	6	6	6	µM	L	6	Inhibition of O_2 for anoxic processes
k_1 OM1	16	16	16	16	16	16	16	16	16	16	yr^{-1}	M		Rate constant for aerobic oxidation of OM1
k_1 OM2	0.1	0.1	0.1	0.1	0.1	0.1	0.1	0.1	0.1	0.1	yr^{-1}	M		Rate constant for aerobic oxidation of OM2
k_2 OM1	5	5	5	5	5	5	5	5	5	5	yr^{-1}	M		Rate constant for denitrification and DNRA of OM1
k_2 OM2	0.1	0.1	0.1	0.1	0.1	0.1	0.1	0.1	0.1	0.1	yr^{-1}	M		Rate constant for denitrification and DNRA of OM2
Adjusted														
k_{nit} 1	90	80	180	180	100	190	20	5	50	60	µmol cm^{-3} yr^{-1}	M		Maximum rate for nitrification step 1
k_{nit} 2	200	195	550	550	400	540	30	50	190	150	µmol cm^{-3} yr^{-1}	M		Maximum rate for nitrification step 2
k_{anx}	0.03	0.05	0.02	0.02	0.04	0.02	0.02	0.02	0.02	0.02	µmol cm^{-3} yr^{-1}	M		Maximum rate for anammox
Measured														
Ø	0.83	0.84	0.88	0.85	0.85	0.82	0.87	0.92	0.59	0.40	cm^3 cm^{-3}	I		Sediment porosity
ρ	2.89	2.49	3.26	2.74	3.08	3.06	2.71	4.45	2.50	1.93	g cm^{-3}	I		Sediment density
T°	11.1	11.9	14.4	14.9	17.9	17.8	16.5	13.8	17.3	15.8	°C	I		Bottom water temperature

The sources of the parameter values are indicated by the following codes: **M**, constrained by the model fitting; **I**, independently determined from the field data, **L**, literature value, with references given as follows: 1. Ward (1986); 2. Wang and VanCappellen (1996); 3. Dalsgaard and Thamdrup (2002); 4. Canavan et al. (2006); 5. Dale et al. (2016); 6. Akbarzadeh et al. (2018).

1361 **Table S4** Model parameter values for the transport processes that were invariable within the season
1362 and sampling station.

Parameters	Value	Description	Unit	Sources
Db	3	Bioturbation coefficient at x < 2 cm	$cm^2\ yr^{-1}$	M
	1.5	Bioturbation coefficient at 2 cm ≤ x ≤ 4 cm	$cm^2\ yr^{-1}$	M
	0.3	Bioturbation coefficient at 4 cm ≤ x ≤ 7 cm	$cm^2\ yr^{-1}$	M
	0.1*(1 - exp(x - 20))	Bioturbation coefficient at x > 7 cm	$cm^2\ yr^{-1}$	M
α	3	Bioirrigation coefficient at x < 2 cm	yr^{-1}	M
	1.5	Bioirrigation coefficient at 2 cm ≤ x ≤ 4 cm	yr^{-1}	M
	0.3	Bioirrigation coefficient at 4 cm ≤ x ≤ 7 cm	yr^{-1}	M
	0.1*(1 - exp(x - 20))	Bioirrigation coefficient at x > 7 cm	yr^{-1}	M
ω	0.5	Burial velocity	$cm\ yr^{-1}$	M

1363 See Table S2 for the source indications
1364

Characteristic time-scales for the sediment processes

1. Diffusion time-scale

Diffusion time-scales calculated from the modified Einstein-Smoluchowski equation (Jørgensen and Revsbech, 1985):

$$t_{DIFF} = z^2/2D_s \quad \text{eq. 1}$$

where t_{DIFF} is the diffusion time-scales (d), z is the characteristic length (cm), and D_s is the diffusion coefficient ($cm^2\ s^{-1}$), corrected with the bottom water temperature and sediment porosity for each measurement. The diffusion time-scale was calculated for the upper 2 cm layer, where the exchange between the sediment and overlying water occurs most actively.

Table S5 Diffusion time-scales for NH_4^+, NO_3^- and DON over the first 2 cm sediment layer.

Date	D_s NH_4^+	D_s NO_3^-	D_s DON*	t_{DIFF} NH_4^+	t_{DIFF} NO_3^-	t_{DIFF} DON
		(x 10^{-6} cm^{-2} s^{-1})			(*d*)	
April 15th.	1.4	1.4	0.17	1.6	1.7	13.2
April 22nd	1.4	1.4	0.18	1.6	1.6	13.2
June 16th	1.5	1.5	0.19	1.5	1.5	12.4
June 24th	1.6	1.5	0.19	1.5	1.5	12.5
August 5th	1.7	1.6	0.21	1.4	1.4	11.3
September 8th	1.7	1.6	0.21	1.4	1.4	11.1

t_{DIFF} = the diffusion time-scale; Ds = the diffusion coefficient. *The D_s of DON was estimated using the empirical relationship between the free solution diffusion coefficient (Do) and the molecular weight (MW) for the various organic compounds at 25°C in distilled water reported by Burdige et al. (1992), assuming a fixed average MW of 2500 Daltons. The obtained values were then corrected for in situ temperature using the Stoke-Einstein equation and translated to Ds after correction for sediment porosity (Boudreau, 1997).

2. Residence time of the solutes

The residence time of the solutes at steady-state can be calculated by dividing the stock of the solutes by the flux of these solutes.

$$t_{RES} = Stock/DifFlux \quad \text{eq. 2}$$

where t_r is the residence time of the solutes (d), *Stock* is the average stock of the solutes over the first 2 cm sediment layer (µmol m^{-2}), and *DifFlux* is the diffusive fluxes of the solutes (µmol m^{-2} d^{-1}).

Table S6 Residence time of NH_4^+, NO_3^- and DON over the first 2 cm sediment layer.

Date	Stock			DifFlux			t_{RES}		
	NH_4^+	NO_3^-	DON	NH_4^+	NO_3^-	DON	NH_4^+	NO_3^-	DON
	(µmol m^{-2})			(µmol m^{-2} d^{-1})			(*d*)		
April 15th.	3,138	376	7,473	427	-247	148	7.4	1.5	50
April 22nd	3,699	294	8,156	541	-99	157	6.8	3.0	52
June 16th	3,487	130	6,471	518	17	175	6.7	7.5	37
June 24th	2,858	198	9,469	439	44	225	6.5	4.5	42
August 5th	3,384	84	6,322	589	21	193	5.7	4.1	33
September 8th	3,795	113	6,916	567	22	212	6.7	5.2	33

* Diffusive fluxes calculated from the concentration gradient at the SWI using Fick's first law of diffusion (Boudreau, 1997; Schulz, 2006)

Sensitivity analysis

The sensitivity analysis was carried out by imposing changes in the model boundary condition (Table S3) and parameter values (Table S2 & S4) for each sampling date. The contribution of NO_2^- to the DIN fluxes was considered negligible (< 5% of the NH_4^+ and NO_3^- fluxes) and therefore it not included in the sensitivity analysis. A stepwise approach was applied by manually changing the parameter values individually (Table S7) and observing the model response on the NH_4^+ and NO_3^- fluxes. The model was run by imposing each change in these values one by one for each sampling date. A combination effect between the parameters was not tested in the sensitivity analysis in the present study. The response was calculated as a percentage of change in the NH_4^+ and NO_3^- fluxes with regard to best fits (baseline model).

Table S7 List of tested parameters for the sensitivity analysis.

Parameters	Description
Anoxic	Bottom water O_2 concentrations are equal to zero
BW NO_3^- = 10x (100x)	Increase in the bottom water NO_3^- concentrations by 10 fold (or 100 fold for August and September)
OM1 2x (3x)	Increase in the deposition of OM1 by 2 fold (or 3x for August)
OM1 <=> OM2	Inversing the proportion of OM1 and OM2
k_1 OM1 = 2x	Increase in the rate constant for the aerobic oxidation of OM1 by 2 fold
k_1 OM1 = 1/2 x	Decrease in the rate constant for the aerobic oxidation of OM1 by one-half
C/N OM1 = 106/16	Imposed change in the C/N ratio compared to that in living phytoplankton (i.e., Redfield ratio)
Db = 10x	Increase in the bioturbation coefficient by 10 fold
α = 10x	Increase in the bioirrigation coefficient by 10 fold

Table S8 Density of macrofauna in the incubated sediment cores (*n = 6*) of the temporal study carried out at the ND monitoring station in 2015.

Taxa / Species names	Apr 15th	Apr 22nd	Jun 16th	Jun 24th	Aug 5th	Sep 8th
Crustacea						
Asthenognathus atlanticus	1	2				
Philocheras bispinosus bispinosus			1			
Echinoderms						
Acrocnida brachiata	1				1	
Amphiura filiformis	6	6	4	22		6
Labidoplax digitata					2	
Leptopentacta elongata			1	2	2	
Synaptidae						
Molluscs						
Abra nitida			1		2	1
Corbula gibba		1				
Kurtiella bidentata	5		1	3		4
Nassarius pygmaeus					1	1
Nucula nitidosa	27	27	15	24	3	5
Philine aperta				1	2	
Spisula solida	1					
Turritella communis				1	1	
Annelids						
Aphelochaeta						1
Chaetozone						1
Glycera unicornis	1					1
Heteromastus filiformis		2				6
Labioleanira yhleni	1	4	2	2	1	
Magelona			1		4	
Maldanidae		1	1	4	1	
Malmgrenia lilianae	3	1		3		
Nephtys	1	1				
Pholoe baltica			1	1		
Sternaspis scutata	5	3	5	1	8	
Cnidaria						
Edwardsidae					1	
Halcampa						
Virgularia					1	4
Others						
Nemertea		2	1			1
Phoronidien		1				1
[a] Average value (Ind. m^{-2})	1354	1328	886	1667	781	833

* Sediment core surface area = 64 cm^2; [a] Average value for 6 sediment cores

Table S9. Spearman's rank correlations between benthic macrofauna density, N transformation rates, benthic N fluxes bottom water turbidity and O_2 concentration for the temporal study in 2015 (n = 6). Asterisks designate significant correlations (∗∗∗ p <0.001, ∗∗ p <0.01, ∗ p <0.05).

	NTF1	NTF2	DNF	DNRA	ANX	AMF	$F.NO_3^-$	$F.NH_4^+$	Fauna	Turb	Oxy
NTF1	1.00										
NTF2	1.00***	1.00									
DNF	-0.49	-0.49	1.00								
DNRA	-0.49	-0.49	1.00***	1.00							
ANX	-0.79	-0.79	0.26	0.26	1.00						
AMF	0.26	0.26	0.43	0.43	-0.53	1.00					
$F.NO_3^-$	0.89*	0.89*	-0.71	-0.71	-0.53	-0.20	1.00				
$F.NH_4^+$	0.23	0.23	0.46	0.46	-0.58	0.99*	-0.23	1.00			
Fauna	-0.31	-0.31	0.66	0.66	-0.18	0.77	-0.66	0.81	1.00		
Turb	-0.90*	-0.90*	0.64	0.64	0.72	-0.12	-0.90*	-0.09	0.29	1.00	
Oxy	-0.03	-0.03	-0.41	-0.41	0.31	-0.93*	0.41	-0.90*	-0.75	-0.13	1.00

NTF1: Nitrification step 1; NTF2: Nitrification step 2; DNF: Denitrification; ANX: Anammox; AMF: Ammonification; $F.NO_3^-$: NO_3^- fluxes; $F.NH_4^+$: NH_4^+ fluxes; Fauna: Macrofauna density: Turb & Oxy: bottom water turbidity (NTU) and oxygen concentration (µM) respectively.

References

Akbarzadeh, Z., Laverman, A.M., Rezanezhad, F., Raimonet, M., Viollier, E., Shafei, B., Van Cappellen, P., 2018. Benthic nitrite exchanges in the Seine River (France): An early diagenetic modeling analysis. Sci. Total Environ. 628-629, 580-593. https://dx.doi.org/10.1016/j.scitotenv.2018.01.319.

Boudreau, B.P., 1997. Diagenetic Models and Their Implementation : Modelling Transport and Reactions in Aquatic Sediments. Springer-Verlag, Berlin.

Burdige, D.J., Alperin, M.J., Homstead, J., Martens, C.S., 1992. The role of benthic fluxes of dissolved organic carbon in oceanic and sedimentary carbon cycling. Geophys. Res. Lett. 19, 1851-1854. https://dx.doi.org/10.1029/92gl02159.

Canavan, R.W., Slomp, C.P., Jourabchi, P., Van Cappellen, P., Laverman, A.M., van den Berg, G.A., 2006. Organic matter mineralization in sediment of a coastal freshwater lake and response to salinization. Geochim. Cosmochim. Ac. 70, 2836-2855. https://dx.doi.org/10.1016/j.gca.2006.03.012.

Cole, T.M., Wells, S.A., 2006. CE-QUAL-W2: A Two-Dimensional, Laterally Averaged, Hydrodynamic and Water Quality Model, Version 3.5. User Manual. p. 680.

Dale, A.W., Sommer, S., Lomnitz, U., Bourbonnais, A., Wallmann, K., 2016. Biological nitrate transport in sediments on the Peruvian margin mitigates benthic sulfide emissions and drives pelagic N loss during stagnation events. Deep Sea Research Part I: Oceanographic Research Papers 112, 123-136. 10.1016/j.dsr.2016.02.013.

Dalsgaard, T., Thamdrup, B., 2002. Factors controlling anaerobic ammonium oxidation with nitrite in marine sediments. Appl Environ Microbiol 68, 3802-3808. https://dx.doi.org/10.1128/aem.68.8.3802-3808.2002.

Jørgensen, B.B., Revsbech, N.P., 1985. Diffusive boundary layers and the oxygen uptake of sediments and detritus1. Limnol. Oceanogr. 30, 111-122. https://dx.doi.org/10.4319/lo.1985.30.1.0111.

Schulz, H.D., 2006. Quantification of Early Diagenesis: Dissolved Constituents in Pore Water and Signals in the Solid Phase. In: Schulz, H.D., Zabel, M. (Eds.), Marine Geochemistry. Springer Berlin Heidelberg, Berlin, Heidelberg, pp. 73-124. https://dx.doi.org/10.1007/3-540-32144-6_3.

Wang, Y.F., VanCappellen, P., 1996. A multicomponent reactive transport model of early diagenesis: Application to redox cycling in coastal marine sediments. Geochim. Cosmochim. Ac. 60, 2993-3014. https://dx.doi.org/10.1016/0016-7037(96)00140-8.

Ward, B.B., 1986. Nitrification in Marine Environments. In: Prosser, J.I. (Ed.), Nitrification. IRL Press, Oxford, pp. 157-184.

1448 **Fig. S1** Sediment core incubations for measuring benthic DIN and DON fluxes in the laboratory.
1449 Two triplicates were incubated in dark and the light conditions, respectively; a control core without
1450 sediment was used to monitor the evolution of the overlying water itself.

1451

1452

Fig. S2 Variations in the salinity and river discharge (Loire and Vilaine) (a, e), temperature and dissolved O_2 (b, f), $NO_3^- + NO_2^-$ and NH_4^+ (c, g), Chl *a* in the water column and sediment surface (d, h), at the Ouest Loscolo monitoring station in 2015 (left) and 2016 (right) from January to December. Dashed-dotted horizontal line (panels a & e): hypoxia threshold (63 µM; Middelburg and Levin, 2009; Zhang et al., 2010). Vertical lines: dates of the sediment investigations.

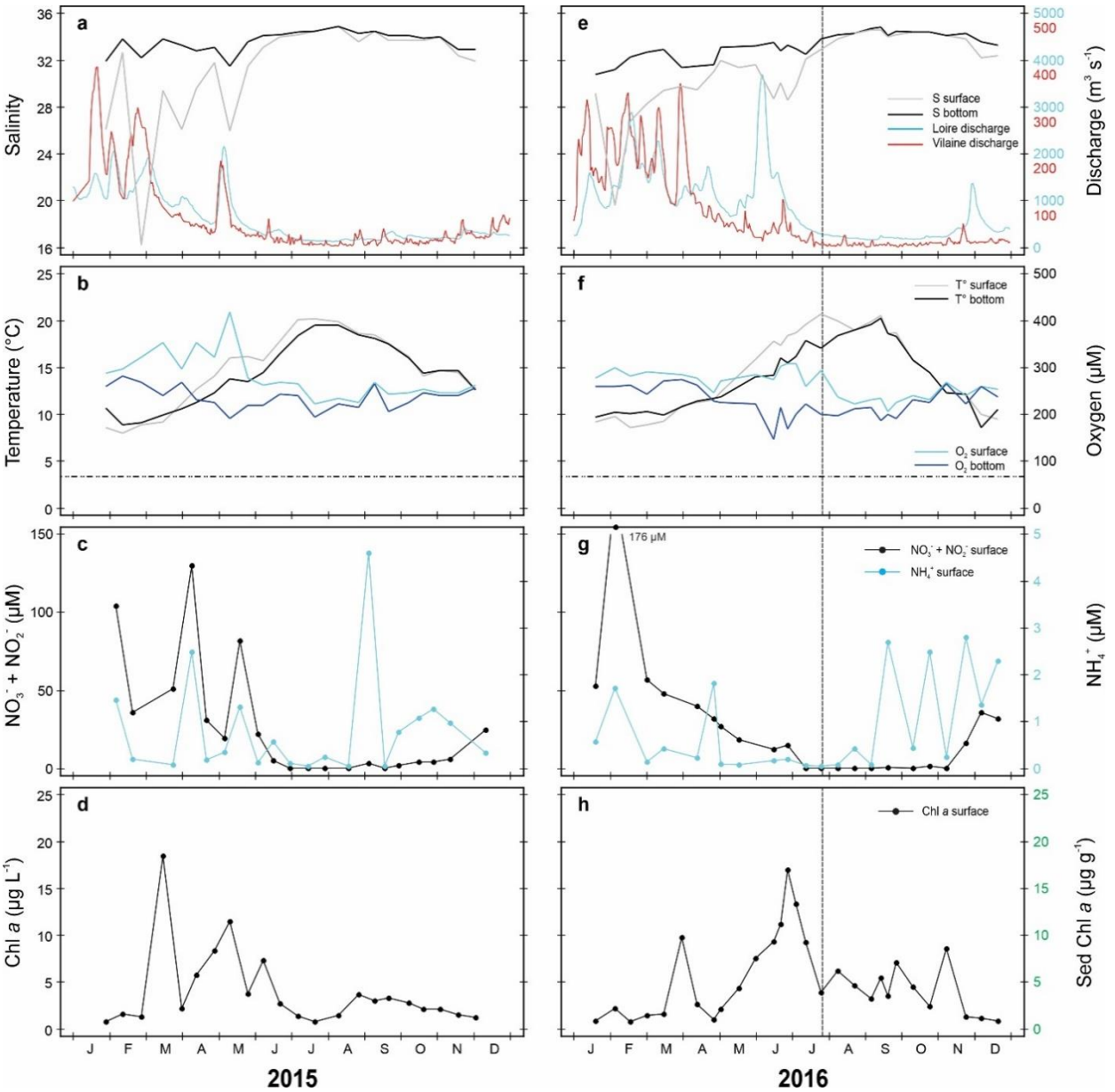

Fig. S3 Depth profile of the grain size distribution at the Nord Dumet monitoring station (St. A) in triplicate sediment cores for the temporal study from April to September 2015. The y-axis represents each section of the sediment layers in the triplicate cores.

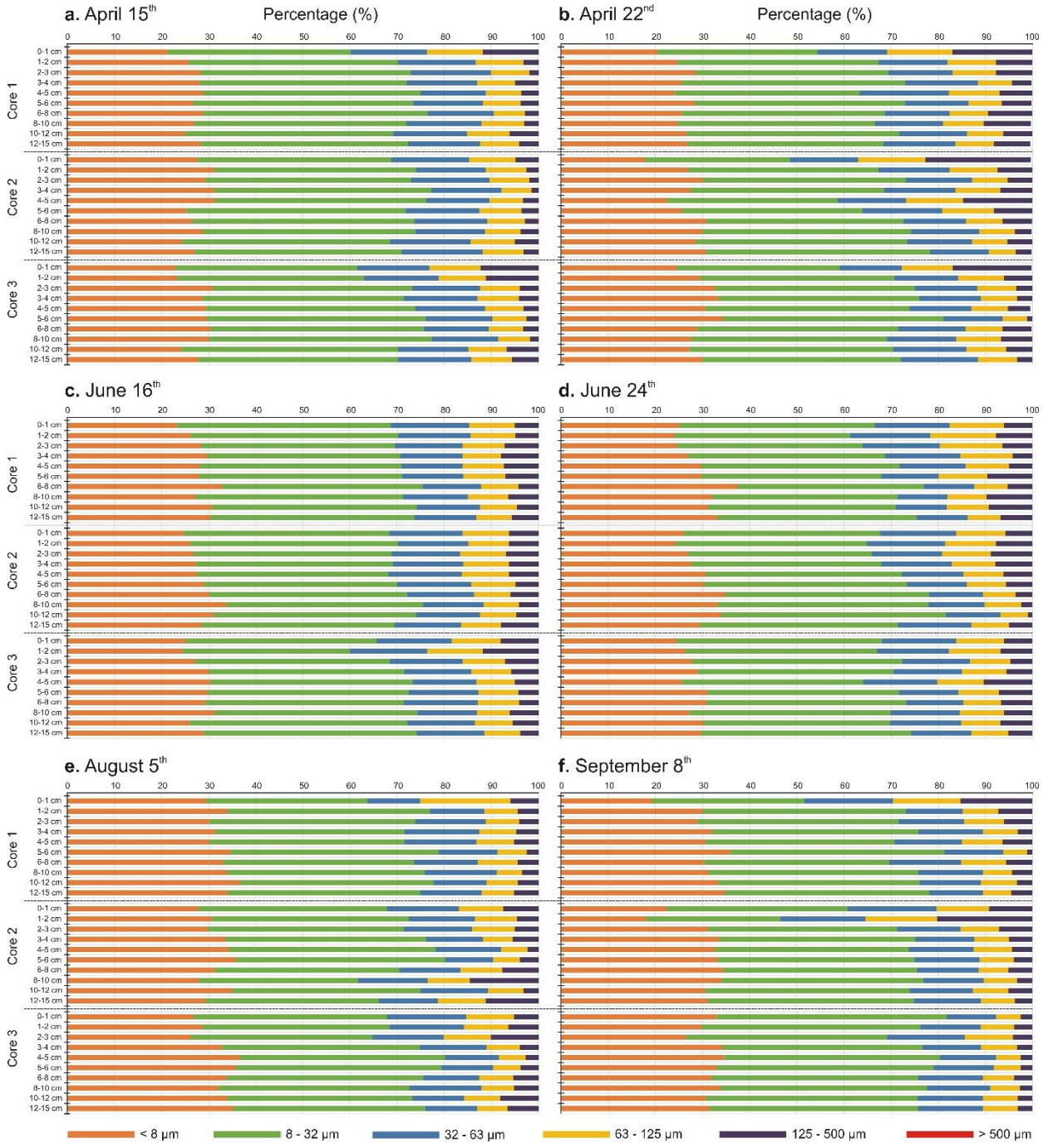

Fig. S4 Depth profile of the grain size distribution in the triplicate sediment cores at Station A, B & C for the spatial study carried out in July 2016. The y-axis represents each section of the sediment layers in the triplicate cores. Right panel: image of a sediment core sampled at Station D. There was no analysis of the grain size distribution for Station D.

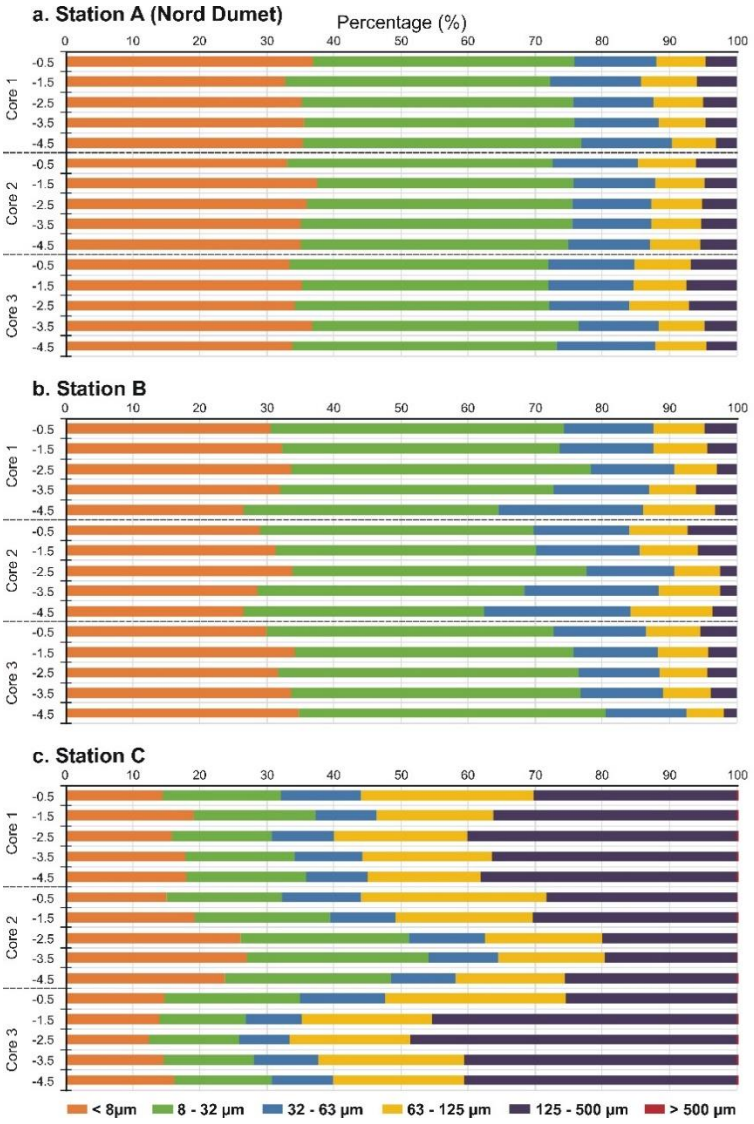

Fig. S5 Depth profiles of the sediment porosity (a) and density (b) at the Nord Dumet monitoring station (St. A) for the temporal study carried out from April to September 2015. The solid horizontal lines are the standard error of the triplicate sediment cores. The red curves are the average of all values with the standard error (*n = 60*).

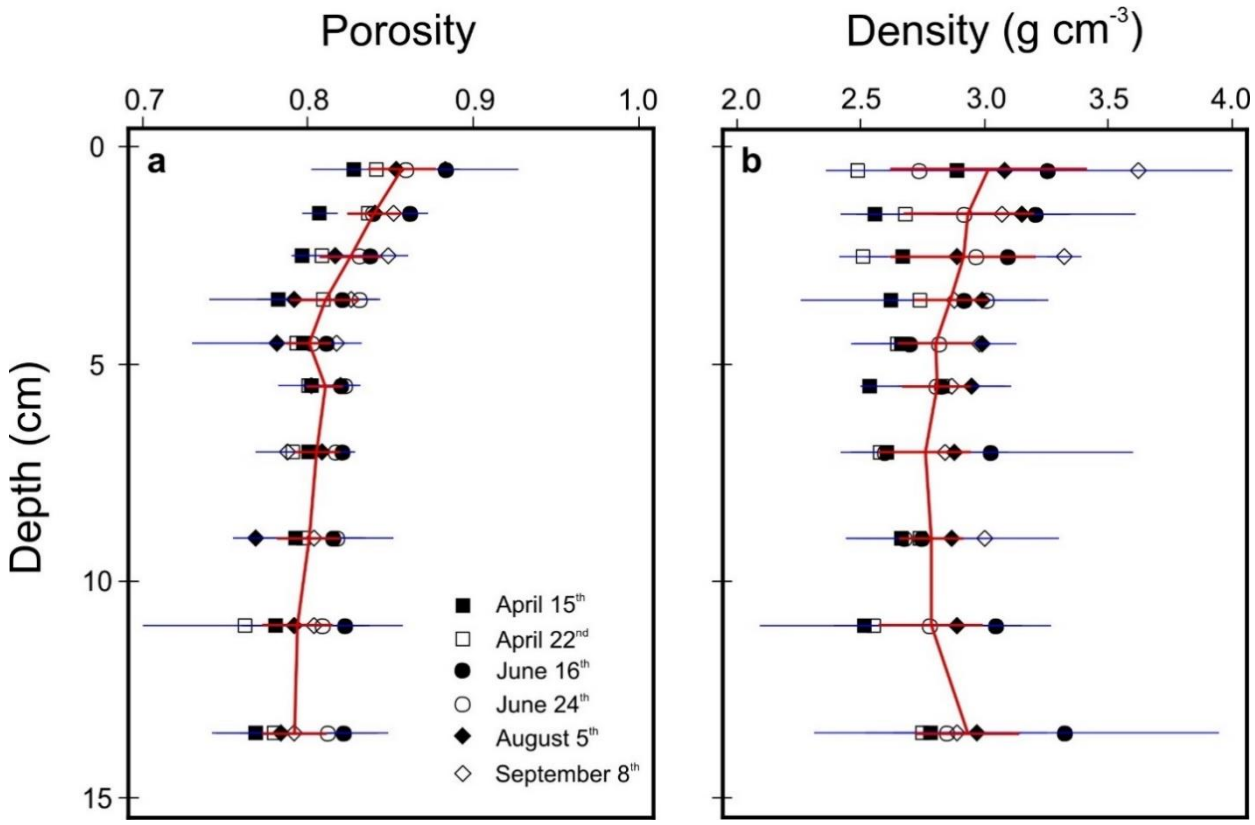

Fig. S6 Depth profiles of the sediment porosity (a) and density (b) at Station A, B & C for the spatial study carried out in July 2016. The solid horizontal lines are the standard error of the triplicate sediment cores. Note: there was no measurement for Station D (gravel).

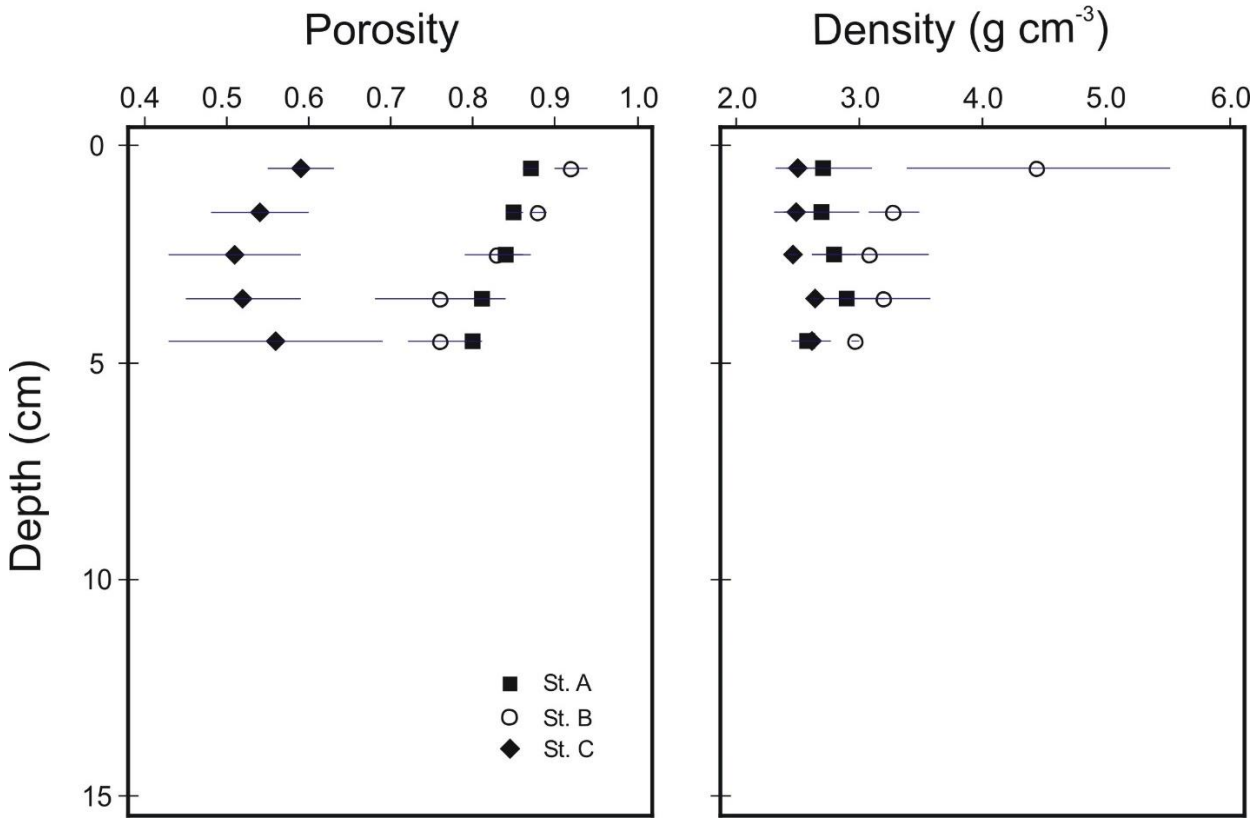

Fig. S7 C_{org}, total N, BSi (in µmol g^{-1}) and Chl *a* (in µg g^{-1}) concentrations at the sediment surface (5 cm and 1 cm for Chl *a*) in April 2016. The data were interpolated using an automatic weighted-average gridding with the Ocean Data View software.

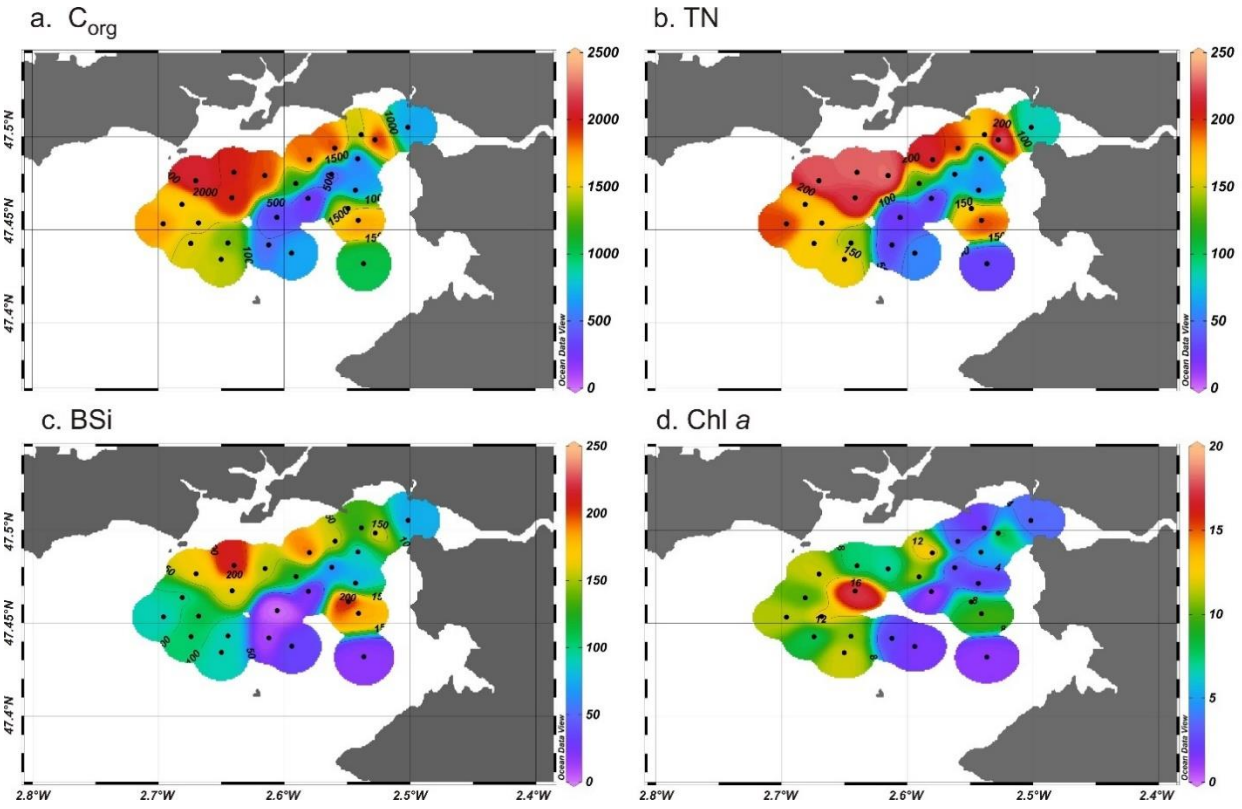

Fig. S8 DON depth profiles at the Nord Dumet monitoring station (St. A) for the temporal study carried out from April to September 2015 (a) and global average of the measured DON and NH_4^+ values (b). The solid horizontal lines are the standard error of the triplicate sediment cores.

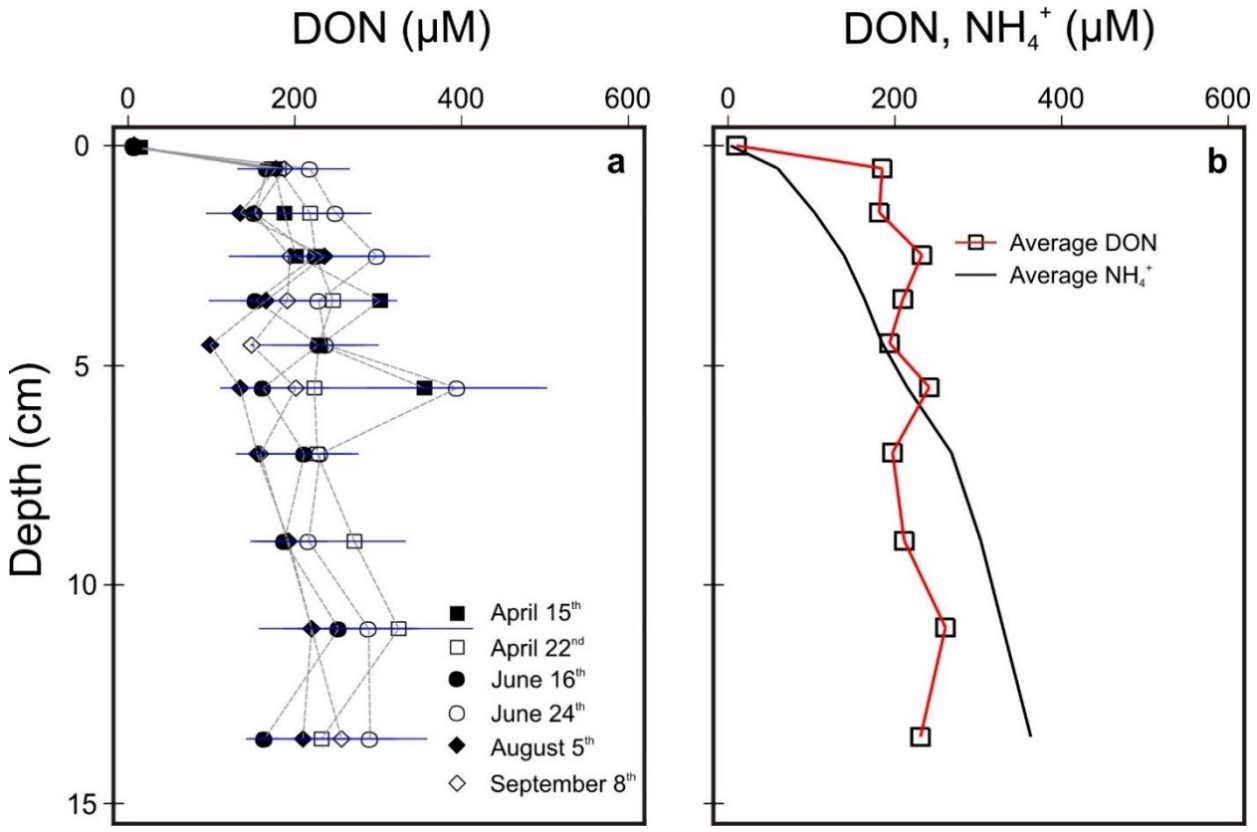

Fig. S9 Microscopic observation of microalgae cells on the surface sediment at the Nord Dumet monitoring station (St. A) during the period of study from April to June (a) and from August to September (b) 2015.

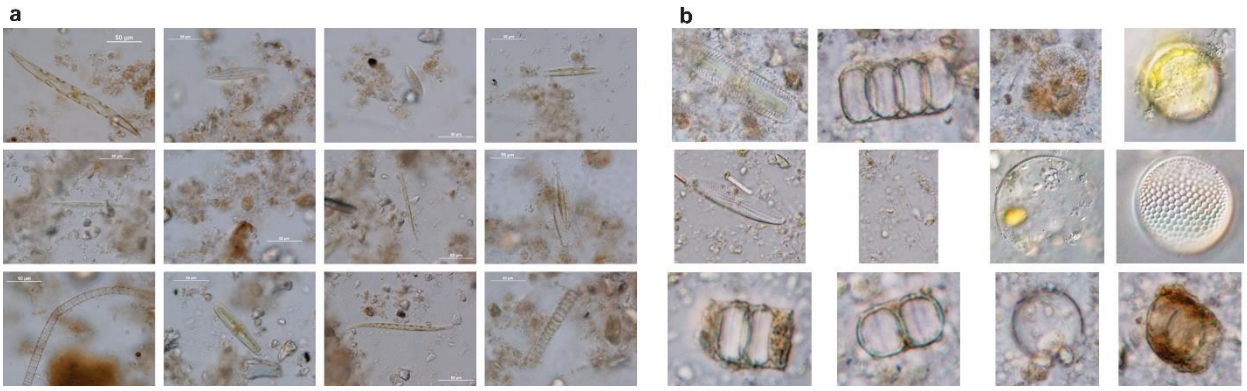

1497

Fig. S10 Modeled NH_4^+ fluxes in 2015 across the SWI as a function of the various *f*DNRA values. Sampling dates are represented by the various colored lines with color symbols. Solid symbols represent the NH_4^+ fluxes measured at the Nord Dumet station.

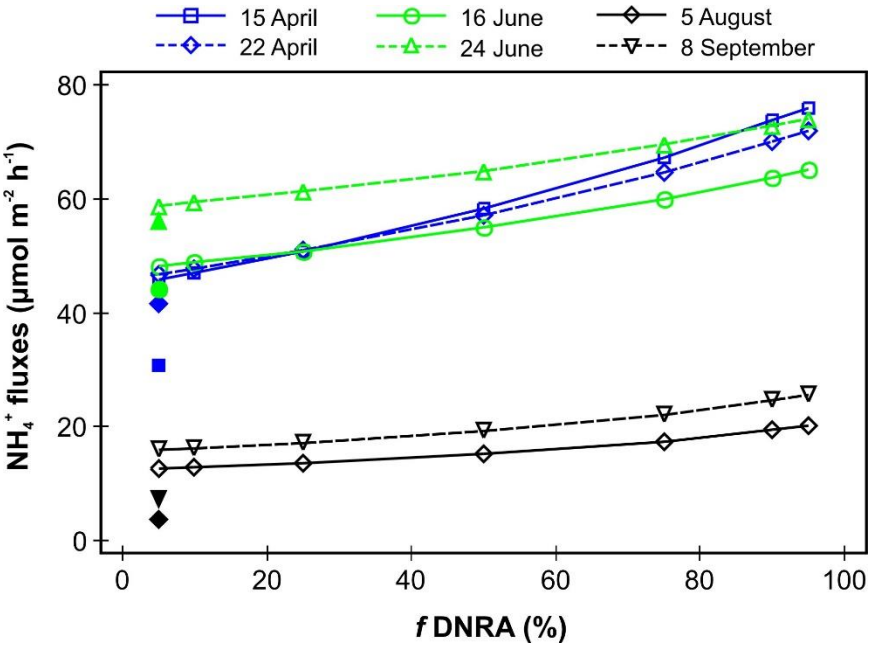

- The temporal and spatial variations of benthic N cycling in a eutrophic macro-tidal bay are studied using field measurements and the reactive transport model

- Benthic N flux variations depend on the phytoplankton-derived organic matter input

- Rapid mineralization of organic matter at the sediment-water interface controls benthic N cycling dynamics and sediment oxygen consumption

- Organic matter decomposition can be followed by bottom water hypoxia when blooms occur in the summer

Declaration of interests

☒ The authors declare that they have no known competing financial interests or personal relationships that could have appeared to influence the work reported in this paper.

☐The authors declare the following financial interests/personal relationships which may be considered as potential competing interests: